minerals

MDPI

Article

Mineralogy of a High-Temperature Skarn, in High CO_2 Activity Conditions: The Occurrence from Măgureaua Vaţei (Metaliferi Massif, Apuseni Mountains, Romania)

Ştefan Marincea [1,*], Delia-Georgeta Dumitraş [1], Cristina Sava [1], Frédéric Hatert [2] and Fabrice Dal Bo [2]

[1] Department INI, Geological Institute of Romania, 1 Caransebeş Str., RO-012271 Bucharest, Romania; d_deliaro@yahoo.com (D.-G.D.); ghinet.cristina@yahoo.com (C.S.)

[2] Laboratoire de Minéralogie, Université de Liège, Sart-Tilman, Bâtiment B 18, B-4000 Liège, Belgium; fhatert@uliege.be (F.H.); fabrice.dalbo@gmail.com (F.D.B.)

* Correspondence: marincea@igr.ro or smarincea@yahoo.com

Received: 19 June 2020; Accepted: 22 July 2020; Published: 30 July 2020

Abstract: A shallow-level monzodioritic to quartz-monzodioritic pluton of the Upper Cretaceous age caused contact metamorphism of Tithonic–Kimmeridgian reef limestones at Măgureaua Vaţei (Metaliferi Massif, Apuseni Mountains, Romania). The preserved peak metamorphic assemblage includes gehlenite (Ak 33.64–38.13), monticellite, wollastonite-2*M*, Ti-poor calcic garnet, and Ca-Tschermak diopside (with up to 11.15 mol.% Ca-Tschermak molecule). From the monzodioritic body to the calcitic marble, the periplutonic zoning can be described as: monzodiorite/agpaitic syenite-like inner endoskarn/wollastonite + perovskite + Ti-poor grossular + Al-rich diopside/wollastonite + Ti-poor grossular + diopside + vesuvianite/gehlenite + wollastonite + Ti poor grossular + Ti-rich grossular (outer endoskarn)/wollastonite + vesuvianite + garnet (inner exoskarn) / wollastonite + Ti-rich garnet + vesuvianite + diopside (outer exoskarn)/calcitic marble. Three generations of Ca garnets could be identified, as follows: (1) Ti-poor grossular (Grs 53.51–81.03 mol.%) in equilibrium with gehlenite; (2) Ti-rich grossular (Grs 51.13–53.47 mol.%, with up to 19.97 mol.% morimotoite in solid solution); and (3) titanian andradite (Grs 32.70–45.85 mol.%), with up to 29.15 mol.% morimotoite in solid solution. An early hydrothermal stage produced retrogression of the peak paragenesis toward vesuvianite, hydroxylellestadite (or Si-substituted apatite), clinochlore, "hibschite" (H_4O_4-substituted grossular). A late hydrothermal event induced the formation of lizardite, chrysotile, dickite, thaumasite, okenite and tobermorite. A weathering paragenesis includes allophane, C-S-H gels and probably portlandite, unpreserved because of its transformation in aragonite then calcite. Overprints of these late events on the primary zoning are quite limited.

Keywords: high-temperature skarn; mineral data; structures; gehlenite; wollastonite-2*M*; monticellite; diopside; vesuvianite; superposed parageneses; Măgureaua Vaţei; Romania

1. Introduction

The high-temperature skarn occurrence from Măgureaua Vaţei (Metaliferi Massif, Apuseni Mountains, Romania) represents one of the very rare occurrences of high-temperature calc-skarns in the world. Fewer than forty records of such rocks, produced by pyrometamorphism [1] were mentioned to date by various authors (e.g., [1–4] and references therein).

The occurrence at Măgureaua Vaţei is known for more than three decades [5] as the most spectacular occurrence of gehlenite worldwide [6]. After the initial description of the occurrence [5], additional mineralogical investigations of the Măgureaua Vaţei skarn were done, but are quite brief, generally referring only to specific mineral species, e.g., gehlenite [6], monticellite [7], clinopyroxene [8]. While the petrographic descriptions were more thorough (i.e., [4]), there remains a paucity of data about the composition, optics and crystallographic parameters of the associated phases, and no structure determinations were carried out, in spite of the well-known tendency for polytypism and lowering symmetry of minerals such as garnets [9–11], wollastonite [12] or vesuvianite [13,14] in high-temperature skarns. This paper aims to bring new and desirable information on the crystal chemistry, physical properties, crystallographic parameters and crystal structures of the main mineral species identified so far in the skarn area. The relative paucity of mineral associations and the large dimensions of the skarn minerals from Măgureaua Vaţei, as compared with the minerals from the two other occurrences of high temperature skarns in Romania (i.e., Cornet Hill and Oraviţa, described by [15–17], respectively), were an advantage for this study.

2. Geological Setting

The occurrence of high-temperature skarn from Măgureaua Vaţei is located at some 7 km south-southwest from the locality Vaţa Băi, and at approximately 20 km west of Brad (which is the closest city in the area). The skarn area is developed at the immediate contact of a mainly quartz-monzodioritic intrusion with Mesozoic limestones (Figure 1).

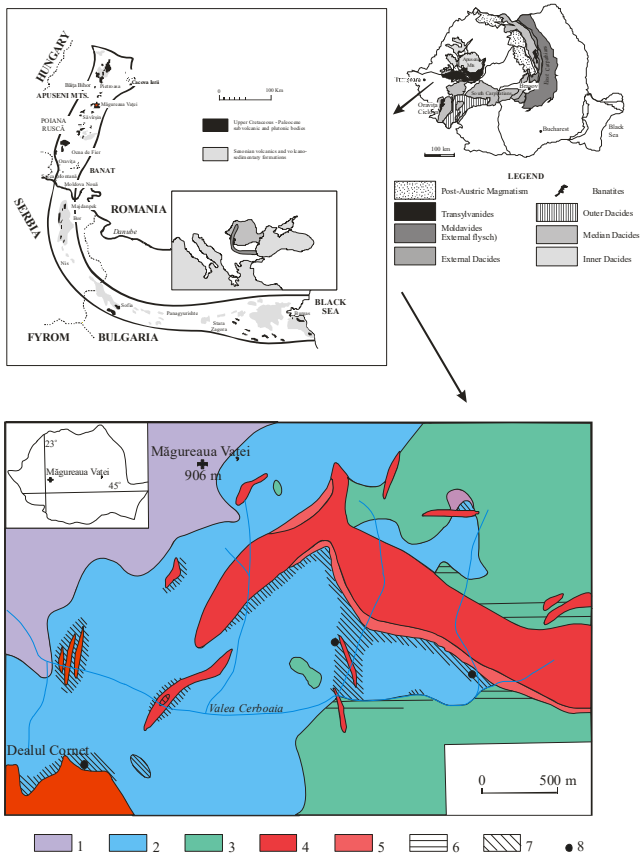

Figure 1. Geological sketch of Măgureaua Vaţei zone (redrawn and modified from [5]) in the regional context: the Banatitic Magmatic and Metallogenetic Belt (top, left: redrawn from [18]) and the structural context of Romania (top, right: redrawn and simplified from) [19]. Symbols in the legend represent: 1—Mesozoic ophiolites; 2—Tithonic–Neocomian limestones (marbles); 3—Senonian clays, sandstones and conglomerates; 4—Quartz monzonites; 5—Monzonites; 6—Pyroxene hornfels; 7—Skarns; 8—Gehlenite occurrences.

The intrusion from Măgureaua Vaţei is among the most basic of the banatitic suite in the area, pertaining to the so-called "Banatitic Magmatic and Metallogenetic Belt" [20]: an extensive suite of consanguineous magmatic and metallogenetic events extended from Srednogorie (Bulgaria) to the Apuseni Mountains (Romania) (Figure 1). For additional information on this important magmatic and metallogenetic province in Europe the reader is referred to [20–22].

The intrusion at Măgureaua Vaţei consists largely of quartz-monzodiorite and monzodiorite with subordinate granodiorite and quartz monzonite, and was emplaced at shallow crust levels during the second of the three cycles of the banatitic evolution in the Apuseni area [23]. Marginal facies of syenite may be interpreted as metasomatic products (i.e., inner endoskarns or "contaminated" rocks: [4,22]), and has the composition of peralkaline (agpaitic) magmas [24]. K-Ar ages range between −75(3) Ma and −61(3) Ma for granodiorites of the Vaţa (Birtin) intrusion [25,26].

The protolith of the high-temperature skarns in the area consists of micritic reef limestones with clastic interlayers. No fossils have yet been identified from this limestone, but certain lithological characteristics reinforce the correlation with similar limestone sequences from the Drocea Mountains [27] and accounts for the Tithonic–Kimmeridgian age.

Everywhere along the intrusive contact the sedimentary rocks are metamorphosed to calc-silicate hornfels and medium- to coarse-grained marble with intercalated bodies of skarn, usually garnet-, wollastonite- and vesuvianite-bearing. A small area of unusual gehlenite-bearing skarn, occurring at the southern central side of the body, on Cerboaia Valley, was studied in greater detail [4–6,8].

The succession of mineral associations from monzodiorite to the calcitic marble defines a well-expressed metasomatic zoning [5], characterized by prograde mineral zones developed at the contact. The zoning, from the inner to the outer part of skarn zone is described as: monzodiorite/gehlenite + garnet ± vesuvianite/garnet + gehlenite + wollastonite/wollastonite + garnet/marble [5]. In the original description [5] the skarn zones are referred to as A, B and C zones. In fact, the zoning is more complex and may be described as follows: monzodiorite/agpaitic syenite-like inner endoskarn/grossular + wollastonite + minor (Al-rich) diopside (inner endoskarn)/gehlenite + wollastonite + garnet + minor monticellite (outer endoskarn)/wollastonite + vesuvianite + garnet (inner exoskarn)/wollastonite + Ti-rich garnet + vesuvianite + diopside (outer exoskarn) [4,8]. The endoskarn may be divided in three sub-zones [4], as follows: wollastonite + perovskite + Ti-poor grossular + Al-rich diopside (A1)/wollastonite + Ti-poor grossular + diopside + vesuvianite (A2)/gehlenite + wollastonite + Ti poor grossular **I** + Ti-rich grossular (A3). The skarn zones could be referred to as A1, A2, A3, B, C1 and C2 zones, respectively (Figure 2).

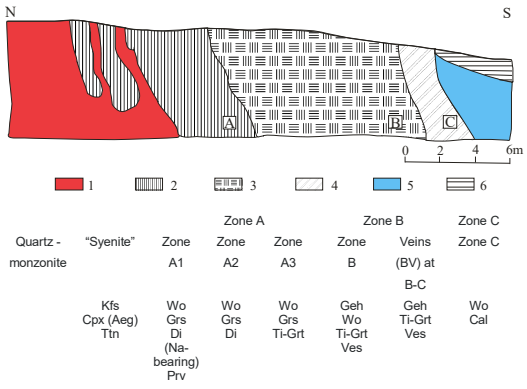

Figure 2. Geological cut of the high-temperature skarn outcrop on the upper Cerboaia Valley (redrawn from [5]). Symbols represent: 1—Quartz monzonite; 2—A zone (gehlenite + vesuvianite + garnet); 3—B zone (garnet + gehlenite + wollastonite); 4—C zone (wollastonite + garnet); 5—Limestone; 6—Diopside hornfels. The mineralogical zoning in the skarn from Măgureaua Vaţei as given by [4] is presented on the bottom. Abbreviations represent: Kfs = alkali feldspar; Cpx (Aeg) = clinopyroxene (aegirine); Ttn = (titanite); Wo = wollastonite; Grs = grossular; Di = diopside; Prv = perovskite; Ti-Grt = titanian garnet; Geh = gehlenite; Ves = vesuvianite; Cal = calcite.

The boundary between B and C1 zones consists of a vein of up to 1 m in width composed of a coarse gehlenite + Ti-rich grossular assemblage, with scarce inclusions of vesuvianite [4]. For simplicity, we use the notation of [5] as modified by [4] for describing the zones. Everywhere, diopside, vesuvianite and hydroxylellestadite (or rather a Si-substituted hydroxylapatite) are minor phases and monticellite is rare. Hydroxyl-bearing or hydrated Ca silicates such as "hibschite", dickite, clinochlore, lizardite, okenite, tobermorite and allophane also occur, as late hydrothermal or weathering products.

3. Materials and Methods

Analyses of material from Măgureaua Vaţei were done using a combination of electron microprobe analysis (EMPA), scanning electron microscopy (SEM), X-ray powder diffraction (XRD), single crystal X-ray diffraction (SCXRD), optical microscopy and cathodoluminescence (CL). More detailed descriptions of analytical procedures used for EMPA, XRD and CL were given by [6,15,17].

EMP analyses were performed using the same devices and operating conditions as described by [6,15]. Data were reduced using the method described by [28]. Supplementary analyses were performed using a CAMECA SX 50 microprobe, hosted at the University in Mons (Belgium), set at an accelerating voltage of 15 kV and a beam current of 20 nA, for a beam diameter of 10 μm. Natural wollastonite (Si and Ca Kα), rutile (Ti Kα), sapphirine (Al Kα), periclase (Mg Kα), hematite (Fe Kα), rhodonite (Mn Kα), leucite (K Kα), oligoclase (Na Kα) and synthetic LiF (F Kα) served as standards. The content of each constituent given in the tables of compositions is an average of N analyses at a given spot on the same thin section.

Part of the X-ray powder-diffraction (XRD) analysis was performed on a Siemens D-5000 Kristalloflex (manufactured by Siemens, Munich, Germany) automated diffractometer equipped with a graphite diffracted-beam monochromator (Cu*K*α radiation, λ = 1.54056 Å.). The operating conditions were the same as described by [15]. Some other analyses were performed using two Brucker (AXS) D8 Advance diffractometers (manufactured by Bruker, Karlsruhe, Germany), in the same operating conditions. In both cases, synthetic silicon (NBS 640b) was used as an external standard, in order to verify the accuracy of the measurements. The unit-cell parameters were calculated by least-squares refinement of the XRD data, using computer programs as described by [29,30], respectively. Part of the X-ray powder data is given as supplementary materials (Tables S1–S8). The full set of data is available from the first author upon request.

The structures of gehlenite, garnet, vesuvianite and wollastonite were refined using X-ray single-crystal diffraction. Data collection of the scattered intensities of X-ray radiation was accomplished on a Agilent X Calibur EOS diffractometer (manufactured by Agilent, Wrocław, Poland), set at 40 kV and 40 mA, with graphite-monochromatized Mo*K*α radiation (λ = 0.71073 Å). The data sets were corrected for Lorentz and polarization effects. Data reduction and analysis were carried out using the CrysAlis PRO routine [31]. The structures were solved by direct methods and refined using the SHELX97 [32] and OLEX 2 [33] programs. The input data were adapted from [34].

Cathodoluminescence analyses were performed on thin sections using a Technosyn 8200 Mark II cold-cathode electron gun (manufactured by Technosyn Limited, Cambridge, UK mounted on a polarizing microscope. The electron beam was accelerated at 10–15 kV, with a 400–500 mA beam current.

The optical properties and indices of refraction were determined using a conventional JENAPOL-U petrographic microscope with a spindle stage, Cargille or temperature-calibrated immersion liquids, and a 589-nm interference filter.

The density of a sample of monticellite was measured by suspension in a solution of Clerici liquid diluted with toluene, whereas the density of four separate vesuvianite clusters was determined using a Berman balance and toluene as displacement fluid, at 20 °C.

4. Mineralogy

4.1. Gehlenite

As stated before, gehlenite was one of most studied minerals in the high-temperature skarns from Măgureaua Vaței (e.g., [4–6,8]). The mineral occurs in practically monomineralic blocks, in the outer endoskarn zone from Cerboaia Valley contact. In the classical outcrop described by [5,6], the crystals, with a short prismatic to tabular habit, may reach up to 8 cm across. A macroscopic image of a gehlenite aggregate from this famous outcrop is given in Figure 3, whereas a microscopic image is given in Figure 4A.

Gehlenite crystals consist of tetragonal prisms {100} simply terminated with {001} pinacoids. A more extensive description was offered by [6], who gives chemical, crystallographic and physical data.

(**A**)

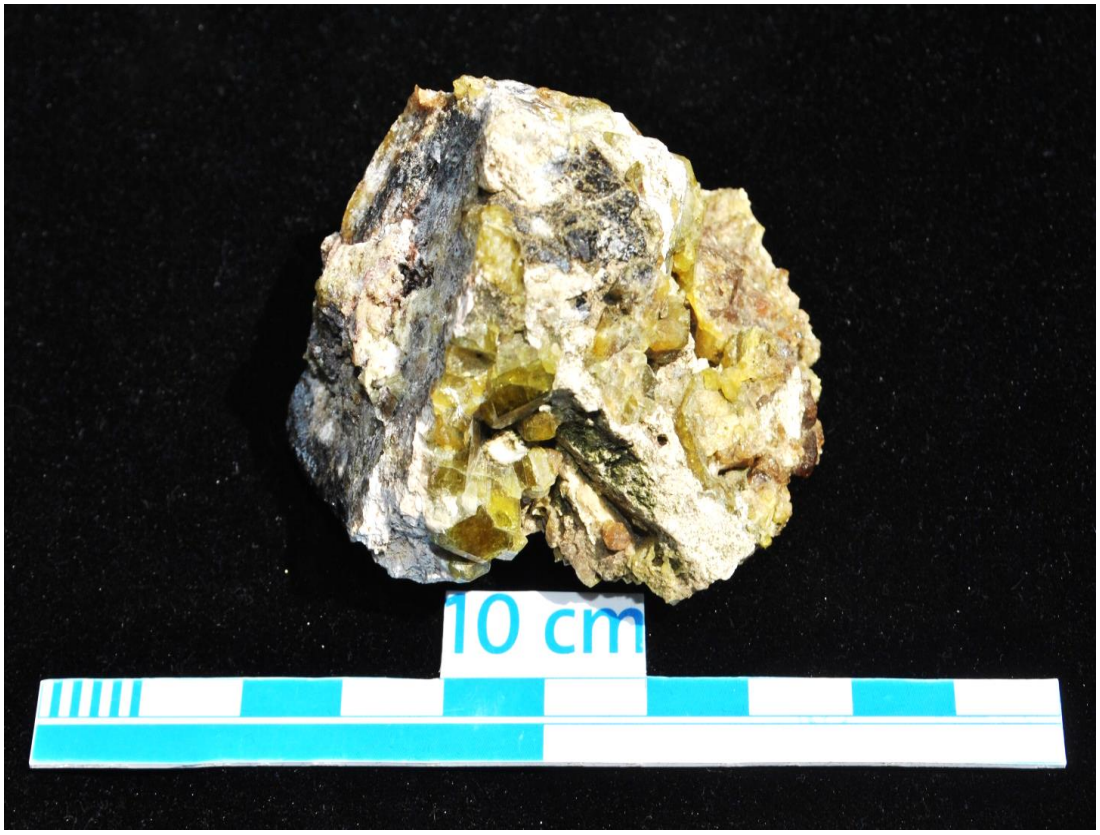

(**B**)

Figure 3. Macrophotographs of a specimen of blocky gehlenite from Măgureaua Vaţei with recognizable tetragonal prism {100} and pinacoid {001} forms (**A**) and of a hand specimen of skarn with vesuvianite crystals showing tetragonal pyramid and basal pinacoid forms (**B**).

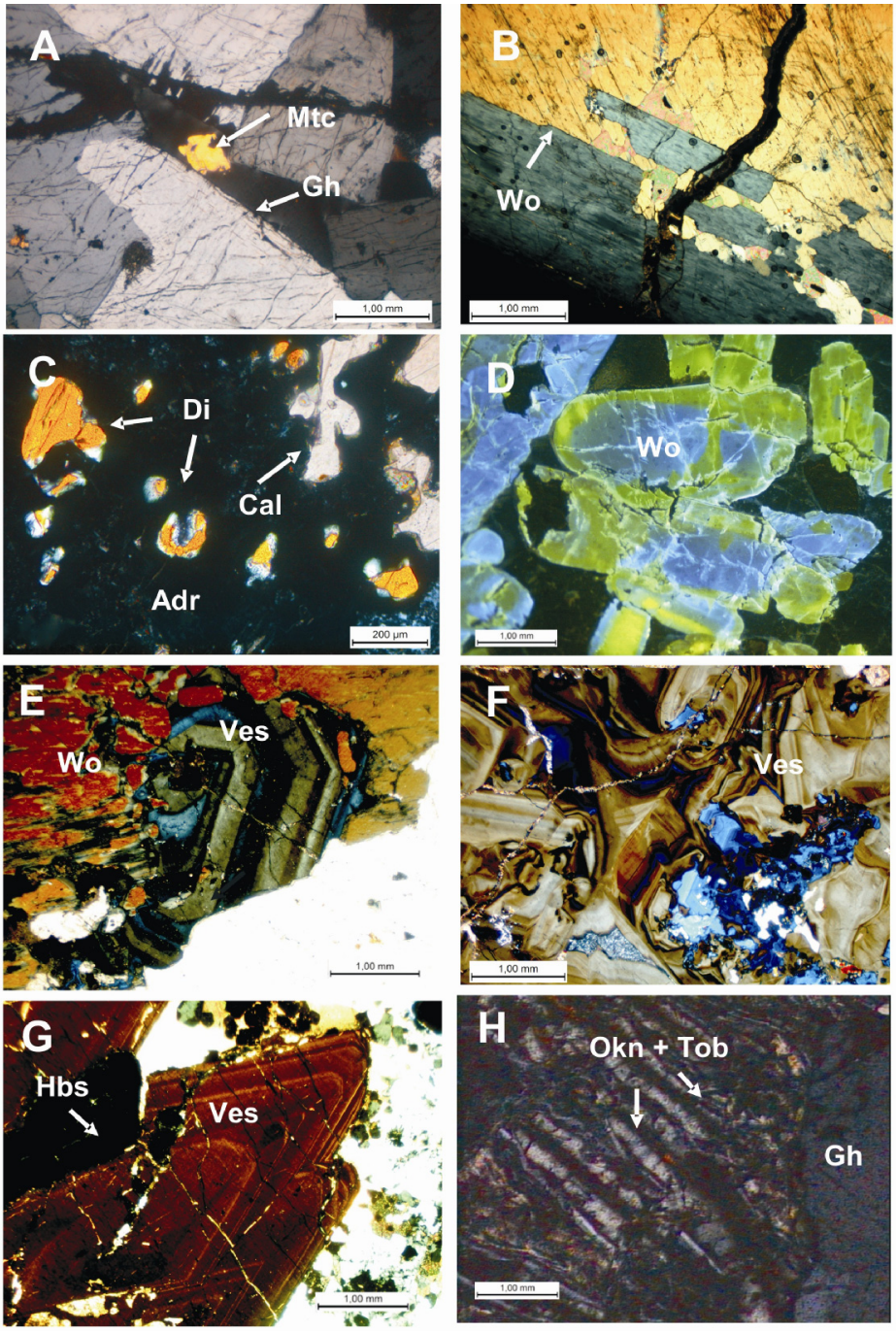

Figure 4. Photomicrographs showing characteristic relationships between minerals in the Măgureaua Vaţei skarn. (**A**) Crystal of monticellite (Mtc) engulfed by gehlenite (Gh). Sample Cer-G-5-069, B zone, crossed polars.); (**B**) Mass of wollastonite-2*M* (Wo). Sample CE005-c, C zone, crossed polars; (**C**) Crystals of diopside (Di) and pads of calcite (Cal) in the Ti-andradite (Adr) mass. Sample Cer-G-5-018, A 1 zone, crossed polars; (**D**) Cathodoluminescence photomicrograph showing zoning in wollastonite (Wo) crystals. Sample 2292, C zone; (**E**) Zoned vesuvianite (Ves) in the wollastonite (Wo) mass. Sample CE0058-f, B zone, crossed polars; (**F**) Zoned and brecciate vesuvianite (Ves). Sample Cer-W-6-002. BV zone, crossed polars; (**G**) "Hibschite" (Hbs) on the fractures of optically zoned vesuvianite (Ves) crystals. Sample 2161, B zone, crossed polars. (**H**) Aggregates of okenite (Okn) and tobermorite (Tob) on a fissure affecting the gehlenite (Gh) mass. Sample CE 4 b, B zone, crossed polars. When possible, symbols of the rock-forming minerals after [35].

For the analyzed samples, the contents of åkermanite in solid solutions range from Ak 30.36 to Ak 42.88 (mean Ak 38.29). The Na-melilite substitution is minor, averaging 2.38 mol.% $CaNaAlSi_2O_7$, whereas the percentages of Fe-åkermanite are low, ranging from 2.21 to 8.61 mol.% (average 5.24 mol.%): [6]. Representative sets of cell parameters are given in Table 1.

Table 1. Crystallographic parameters of selected minerals in the Măgureaua Vaţei skarns.

Mineral Species	Space Group	Sample	*a* (Å)	*b* (Å)	*c* (Å)	*β*(°)	*V* (Å^3)	n (1)	N (2)	2θ (3)
gehlenite	$P\bar{4}2_1m$	P 4	7.718(3)	-	5.049(2)	-	300.7(1)	6	40	10–80
gehlenite	$P\bar{4}2_1m$	P 27*	7.683(4)	-	5.063(3)	-	298.8(3)	3	40	10–80
gehlenite	$P\bar{4}2_1m$	P 49	7.690(3)	-	5.060(2)	-	299.2(2)	3	41	10–80
gehlenite	$P\bar{4}2_1m$	1509	7.713(2)	-	5.043(1)	-	300.0(1)	9	44	10–80
gehlenite	$P\bar{4}2_1m$	1519	7.693(3)	-	5.070(3)	-	300.0(2)	6	49	10–80
gehlenite	$P\bar{4}2_1m$	2125	7.735(1)	-	5.040(1)	-	301.5(1)	10	48	10–80
gehlenite	$P\bar{4}2_1m$	2128	7.717(2)	-	5.045(1)	-	300.4(1)	10	53	10–80
gehlenite	$P\bar{4}2_1m$	2234	7.687(3)	-	5.063(3)	-	299.2(1)	3	40	10–80
gehlenite	$P\bar{4}2_1m$	2317	7.727(2)	-	5.040(1)	-	300.9(1)	10	48	10–80
gehlenite	$P\bar{4}2_1m$	2318	7.712(2)	-	5.045(1)	-	300.1(1)	7	38	10–80
Ti-andradite	*Ia*3*d*	2304	12.024(6)	-	-	-	1738.2(3)	3	19	20–90
Ti-andradite	*Ia*3*d*	P 27*	12.102(1)	-	-	-	1772.3(5)	10	26	20–90
andradite	*Ia*3*d*	P 30*	12.003(4)	-	-	-	1729.1(9)	3	26	20–90
andradite	*Ia*3*d*	2299	11.923(2)	-	-	-	1694.8(9)	3	22	20–90
grossular	*Ia*3*d*	P 1	11.867(1)	-	-	-	1671.0(6)	4	30	20–90
grossular	*Ia*3*d*	P 5	11.880(2)	-	-	-	1676.8(7)	4	26	20–90
grossular	*Ia*3*d*	1519	11.887(4)	-	-	-	1679.6(2)	10	24	20–90
grossular	*Ia*3*d*	2159*	11.897(1)	-	-	-	1683.9(2)	6	34	20–90
grossular	*Ia*3*d*	2234	11.868(1)	-	-	-	1671.6(6)	8	32	20–90
grossular	*Ia*3*d*	2304	11.874(4)	-	-	-	1673.9(9)	3	20	20–90
grossular	*Ia*3*d*	2317	11.885(3)	-	-	-	1678.7(9)	4	20	20–90
"hibschite"	*Ia*3*d*	2161	11.963(4)	-	-	-	1712.1(9)	5	22	20–90
"hibschite"	*Ia*3*d*	2301	11.953(4)	-	-	-	1707.9(2)	4	23	20–90
monticellite	*Pbnm*	P 4	4.822(2)	11.130(5)	6.384(3)	-	342.6(2)	5	50	5–90
vesuvianite	*P*4/*nnc*	P 6	15.621(3)	-	11.846(3)	-	2890.7(9)	9	71	5–65
vesuvianite	*P*4/*nnc*	1513	15.587(3)	-	11.832(3)	-	2874.7(9)	6	128	5–65
vesuvianite	*P*4/*nnc*	2234	15.575(4)	-	11.814(5)	-	2865.9(9)	5	60	5–65
vesuvianite	*P*4/*nnc*	2293	15.564(8)	-	11.767(9)	-	2850.2(9)	6	50	5–65
vesuvianite	*P*4/*nnc*	2303	15.592(6)	-	11.835(8)	-	2876.2(9)	5	59	5–65
vesuvianite	*P*4/*nnc*	2304	15.581(7)	-	11.832(9)	-	2872.6(9)	3	48	5–65
vesuvianite	*P*4/*nnc*	2335	15.570(5)	-	11.837(7)	-	2869.8(9)	3	66	5–65
wollastonite	*P*2$_1$/*a*	P 5	15.426(2)	7.328(1)	7.069(1)	95.33(1)	795.7(1)	9	81	10–80
wollastonite	*P*2$_1$/*a*	P 6	15.412(5)	7.321(3)	7.075(2)	95.34(2)	794.8(4)	6	81	10–80
wollastonite	*P*2$_1$/*a*	1517	15.415(2)	7.317(1)	7.064(1)	95.36(1)	793.2(1)	10	85	10–80
wollastonite	*P*2$_1$/*a*	2158*	15.416(2)	7.314(1)	7.064(1)	95.37(1)	793.0(2)	10	66	10–80
wollastonite	*P*2$_1$/*a*	2159*	15.416(1)	7.315(1)	7.064(1)	95.36(1)	793.0(8)	10	77	10–80
wollastonite	*P*2$_1$/*a*	2292	15.414(6)	7.318(3)	7.069(4)	95.37(2)	793.8(4)	6	57	10–80
wollastonite	*P*2$_1$/*a*	2299	15.411(4)	7.322(2)	7.065(2)	95.37(2)	793.7(3)	5	72	10–80
wollastonite	*P*2$_1$/*a*	2336	15.406(4)	7.318(2)	7.057(2)	95.37(2)	792.2(2)	8	61	10–80
clinochlore	*C*2/*m*	2303	5.322(6)	9.232(7)	14.318(9)	96.25(5)	699.3(9)	6	58	5–90
calcite	$R\bar{3}c$	2158*	4.988(1)	-	17.056(1)	-	367.5(3)	3	29	20–90
calcite	$R\bar{3}c$	2292	4.990(5)	-	17.076(3)	-	368.2(1)	3	34	20–110
calcite	$R\bar{3}c$	2299	4.986(2)	-	17.065(6)	-	367.4(2)	3	25	20–110

dickite	*Cc*	1519	5.149(2)	8.898(4)	14.504(6)	100.17(2)	654.1(3)	10	86	5–90

* Sample taken from Crămuț Valley; [(1)] number of cycles in the refinement; [(2)] number of reflections used in the refinement; [(3)] range of 2θ angles used in collecting the reflections.

The structural refinement of a representative sample of gehlenite from Cerboaia Valley (Sample CE 4B) was done in order to supplement the data on mineral already furnished [6]. The chemical composition of this sample is (in wt.% oxides): SiO_2 = 30.76, TiO_2 = 0.02, Al_2O_3 = 21.34, FeO = 2.43, CaO = 39.12, MnO = 0.08, MgO = 4.40, Na_2O = 0.47, K_2O = 0.03, Total = 98.65. All iron was considered in divalent state of oxidation. The chemical-structural formula corresponding to this composition as calculated on the basis of 14 (O) *pfu* is:

$(Na_{0.086}K_{0.004}Ca_{3.904})(Al_{1.207}Ti_{0.001}Mn_{0.006}Mg_{0.611}Fe^{2+}_{0.189})(Si_{2.865}Al_{1.135})O_{14}$ indicative for a gehlenite (Gh = 58.92 mol.%) with 29.34 mol.% åkermanite, 8.99 mol.% Fe-åkermanite and 2.75 mol.% Na-melilite in the solid solution, in the trend of those previously analyzed by [6].

A projection of the structure on (001) is given in Figure 5. Data of structure refinement are labeled in Table 2, whereas refined atomic coordinates and site occupancies, anisotropic displacement parameters and selected interatomic distances are listed in Table 3. Structural refinements were successfully performed in the space group $P\bar{4}2_1m$, the same as established by [36]. The structure can be described as a framework of disilicate groups composed of two corner-sharing $[SiO_4]$ tetrahedrons, which are each linked by an O corner to $[AlO_4]$ tetrahedrons to form layers composed by rings of five tetrahedron parallels to (001). The tetrahedral linkage within the structure is similar to that of an aluminosilicate framework structure [36]. Each of the two remaining corners of the $[SiO_4]$ tetrahedrons is bonded to Ca ions that occupy the centers of the tetrahedron rings. Ca^{2+} is coordinated eight-fold, and also ensures the linkage between two successive layers of tetrahedrons.

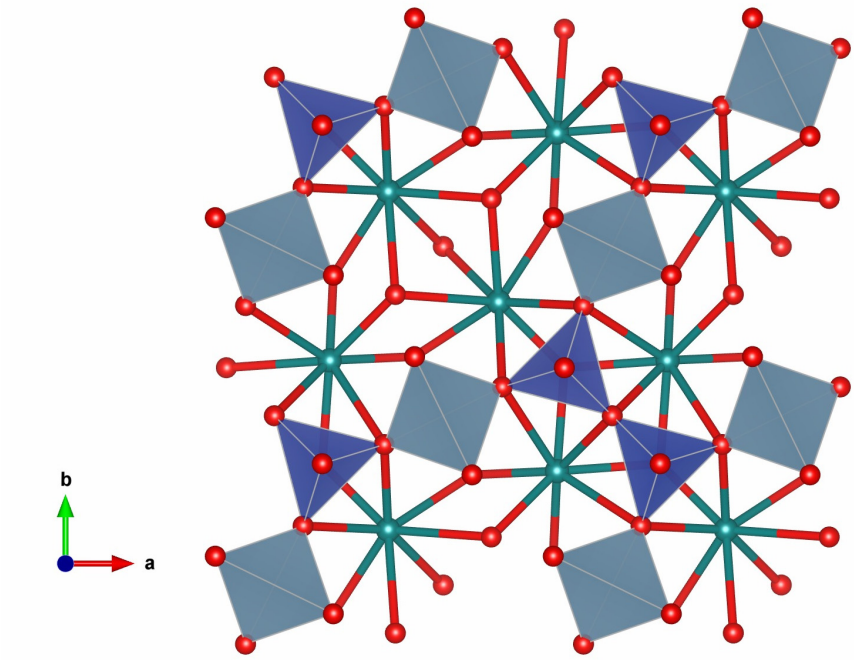

Figure 5. Projection of the structure of gehlenite (sample CE 4 b) along (001). The deep blue tetrahedrons represent SiO_4, the gray blue octahedrons represent AlO_4, the red circles represent O atoms, and the turquoise circles represent the eight-for coordinated Ca atoms.

Table 2. Details of the X-ray data collection and refinements of various mineral species from Măgureaua Vaţei high-temperature skarn.

Mineral Species	Grossular	Ti-Andradite	Gehlenite	Wollastonite	Vesuvianite	Vesuvianite	Vesuvianite
Sample	CE 5B	CE 5C	CE 4B	CE 5B	CE 1A	CE 2A	CE 8A
Crystal shape	idiomorphic	idiomorphic	tabular	tabular-columnar	bipyramidal	bipyramidal	prismatic-bipyramidal
Color	brown	pitch black	gray	white	green	brownish green	brownish green
Crystal size (mm^3)	4 × 4 × 4	8 × 8 × 8	15 × 15 × 10	12 × 20 × 100	8 × 8 × 6	5 × 5 × 4	6 × 6 × 8
a (Å)	11.9218(2)	12.0242(3)	7.7404(3)	15.4206(7)	15.6037(2)	15.5680(3)	15.6351(4)
b (Å)	11.9218(2)	12.0242(3)	7.7404(3)	7.3228(3)	15.6037(2)	15.5680(3)	15.6351(4)
c (Å)	11.9218(2)	12.0242(3)	5.0388(3)	7.0684(3)	11.8388(4)	11.8464(4)	11.7515(5)
β (°)	90.00	90.00	90.00	95.379(4)	90.00	90.00	90.00
V ($Å^3$)	1694.45(6)	1738.48(7)	301.90(2)	794.67(6)	2882.5(1)	2871.1(1)	2872.7(2)
Space group	*Ia*3*d*	*Ia*3*d*	$P\bar{4}2_1m$	$P2_1/a$	*P*4/*nnc*	*P*4/*nnc*	*P*4/*nnc*
Z	8	8	2	9	2	2	2
$D_{calc.}$ (g/cm^3)	4.035	3.909	3.017	2.185	3.246	3.378	3.356
Absorption coefficient (mm^{-1})	5.769	5.613	2.369	1.923	2.543	2.617	2.592
F(000)	2025	2013	272	522	2812	2912	2895
Max. 2ϴ (°)	57.45	57.63	58.07	57.56	57.83	58.05	57.77
Range of indices	−16 ≤ h ≤ 16	−14 ≤ h ≤ 16	−10 ≤ h ≤ 10	−9 ≤ h ≤ 8	−20 ≤ h ≤ 21	−20 ≤ h ≤ 21	−20 ≤ h ≤ 20
	−15 ≤ k ≤ 10	−9 ≤ k ≤ 15	−9 ≤ k ≤ 10	−9 ≤ k ≤ 9	−20 ≤ k ≤ 19	−21 ≤ k ≤ 21	−19 ≤ k ≤ 19
	−15 ≤ l ≤ 15	−14 ≤ l ≤ 15	−6 ≤ l ≤ 6	−20 ≤ l ≤ 20	−14 ≤ l ≤ 15	−16 ≤ l ≤ 15	−10 ≤ l ≤ 15
Number of measured reflections	5369	5591	4140	6002	15,162	58,217	23,371
Number of unique reflections	183	192	427	1868	1821	1878	1843
Number of refined parameters	22	20	36	136	163	163	163
R_1 (*F*) with $F_0 > 4s(F_0)$ *	0.0268	0.0151	0.0212	0.0265	0.0292	0.0377	0.0410
R_1 (*F*) for all the unique reflections *	0.0284	0.0173	0.0232	0.0387	0.0326	0.0391	0.0438
wR_2 (F^2) *	0.0737	0.0479	0.0537	0.0755	0.0770	0.0961	0.1004
S ("goodness of fit")	1.265	1.363	1.247	1.195	1.060	1.359	1.240
Weighing scheme: $\Delta\sigma_{min}$; $\Delta\sigma_{max}$	−0.479; 0.399	−0.184; 0.171	−0.529; 0.319	−0.518; 0.404	−0.743; 3.859	−0.873; 2.255	−0.886; 3.303

* Notes: $R_1 = \Sigma(|F\text{obs}| - |F\text{calc}|)/\Sigma|F\text{obs}|$; $wR_2 = \{\Sigma[w(F^2\text{obs} - F^2\text{calc})2]/\Sigma[w(F^2\text{obs})^2]\}^{0.5}$, $w = 1/[S^2(F^2\text{obs}) + (aP)^2 + bP]$, $P = [\text{Max}(F^2\text{obs},0) + 2F^2\text{calc}]/3$.

Table 3. Structure factors obtained for a selected sample of gehlenite from Măgureaua Vaţei (sample CE 4 B).

Atomic Coordinates and Isotropic Equivalents (U_{eq}) in Å^2.					
Site	**Atom**	***x***	***y***	***z***	U_{eq}
Ca	Ca	0.3365(5)	0.1635(5)	0.5098(12)	0.0185(2)
Si	Si	0.6418(7)	0.1418(7)	0.0520(15)	0.0119(2)
Al	Al	10.000	0.0000	0.0000	0.0127(4)
O2	O	0.6418(2)	0.1418(2)	−0.2709(4)	0.0204(5)
O3	O	0.8254(2)	0.0851(2)	0.2009(3)	0.0222(4)
O1	O	0.5000	0.0000	0.1780(7)	0.0221(7)
Anisotropic Temperature Factors (Å2)					
Site	U_{11}	U_{22}	U_{33}	U_{23}	U_{13}	U_{12}
Ca	0.0213(2)	0.0213(2)	0.0130(3)	−0.0004(1)	0.0004(2)	0.0069(2)
Si	0.0120(3)	0.0120(3)	0.0117(4)	0.0000(2)	0.0000(2)	−0.0009(3)
Al	0.0112(4)	0.0112(4)	0.0158(7)	0.000	0.000	0.000
O1	0.028(1)	0.028(1)	0.010(1)	0.000	0.000	−0.013(1)
O2	0.0206(7)	0.0206(7)	0.020(1)	0.0035(6)	0.0035(6)	−0.004(1)
O3	0.0200(8)	0.0295(9)	0.0171(8)	−0.0053(7)	−0.0041(7)	0.0045(7)
Valency Factors					
Parameter	**Si**	**Ca**	**Al**		
SOF	0.715 Si + 0.285 Al	1.000 Ca	0.600 Al + 0.0305 Mg + 0.095 Fe^{2+}		
M-O th	1.718	2.540	2.620		
M-O meas	1.659	2.567	1.812		
d elec. th	13.72	20.00	35.93		
d elec. meas	14.00	20.00	13.00		
Val th.	3.72	2.00	6.70		
Val meas.	3.72	1.69	369.30		
Selected Interatomic Distances (Å)					
Ca-O(1) × 2	2.449(2)				
Ca-O(2) × 4	2.614(2)				
Ca-O(2) × 2	2.448(2)				
Ca-O(3) × 3	2.433(2)				
Ca-O(3) × 3	2.774(2)				
Mean Ca-O	2.562				
Si-O(1) × 2	1.677(1)				
Si-O(2)	1.627(2)				
Si-O(3) × 2	1.666(2)				
Mean Si-O	1.663				
Al-O(3) × 4	1.812(2)				
Mean Al-O	1.812				

4.2. Calcic Garnets

Three generations of garnet may be recognized on the basis of textural relationships in the skarns from Măgureaua Vaţei, as well as in the high temperature skarn from Cornet Hill [15]. Chemical analyses were carried out for a better characterization of these garnets, and a representative set of electron-microprobe results is given in Tables 4 and 5. The number of ions was calculated on the basis of (Ca + Fe + Ti + Al + Mg + Mn + Na) = 5 *apfu* (atoms per formula unit), as recommended for andradite with a significant hydrogarnet component [37]. This basis for normalization was maintained for all samples, for homogeneity. In Ti-poor samples (Table 4) the Droop method [38] was used to calculate the partition of Fe between Fe^{2+} and Fe^{3+}.

Table 4. Representative compositions of grossular **I**, Măgureaua Vaţei *.

Sample	2297	2303A	2303B	2303 C	P4	P1	P5	CE 5B
Zone	A 1	B	B	B	B	B	BV	BV
N (1)	5	5	3	4	3	4	3	4
SiO_2	37.82	36.31	38.34	37.38	38.77	39.01	39.08	37.95
TiO_2	1.20	0.88	0.14	1.51	0.65	0.68	0.56	0.29
Al_2O_3	15.94	11.55	14.05	11.54	16.92	17.57	18.29	14.72
Cr_2O_3	-	-	-	-	-	-	-	0.01
Fe_2O_3 (2)	7.24	13.99	10.73	12.56	7.50	6.33	5.47	9.90
FeO(2)	1.03	0.77	0.12	1.36	0.55	0.57	0.47	0.25
MnO	0.15	0.07	0.07	0.01	0.14	0.11	0.14	0.11
MgO	0.54	0.21	0.16	0.37	0.48	0.57	0.57	0.11
CaO	35.30	35.29	36.66	34.76	35.67	35.79	36.00	36.25
Na_2O	0.01	0.00	0.00	0.02	0.01	0.01	0.01	0.01
Total	99.23	99.07	100.27	99.51	100.69	100.64	100.59	99.60
Number of Cations on the Basis of 5 (Ca + Fe + Ti + Al + Mg + Mn + Na + K)								
Si	2.927	2.859	2.977	2.959	2.957	2.967	2.962	2.952
Ti	0.070	0.052	0.008	0.090	0.037	0.039	0.032	0.017
Al	1.454	1.072	1.286	1.077	1.521	1.575	1.634	1.349
Cr	-	-	-	-	-	-	-	0.001
Fe^{3+}	0.476	0.870	0.633	0.748	0.445	0.376	0.335	0.592
Fe^{2+}	0.000	0.000	0.000	0.090	0.017	0.020	0.002	0.000
Mn	0.010	0.005	0.005	0.001	0.009	0.007	0.009	0.006
Mg	0.062	0.025	0.019	0.044	0.055	0.065	0.064	0.013
Ca	2.927	2.977	3.050	2.948	2.915	2.917	2.923	3.021
Na	0.002	0.000	0.000	0.003	0.001	0.001	0.001	0.001
O	11.889	11.742	11.923	11.920	11.934	11.948	11.940	11.892
$(OH)^-$ (3)	0.222	0.516	0.155	0.160	0.133	0.104	0.120	0.217
$(OH)^-$ (4)	0.292	0.564	0.092	0.164	0.172	0.132	0.152	0.192
Composition in Terms of End-Members (mol.%) (5)								
Grs	72.28	53.51	66.20	56.05	75.14	78.32	81.03	68.44
Adr	23.80	43.63	32.85	39.06	22.22	18.89	16.74	30.22
Uv	-	-	-	-	-	-	-	0.01
Mrm	3.50	2.61	0.42	4.70	1.85	1.96	1.60	0.87
Prp	0.32	0.16	0.40	0.18	0.41	0.46	0.50	0.32
Alm	0.00	0.00	0.00	0.00	0.29	0.30	0.04	0.00
Sps	0.10	0.09	0.14	0.00	0.08	0.06	0.10	0.10

* Results expressed in wt.%; (1) number of point analyses; (2) as deduced from total iron (see text); (3) as deduced from the O^{2-} contents, for $[O + (OH)_2] = 12$ *apfu*; (4) as deduced from the Si contents, for $[Si + (OH)_4] = 3$ *apfu*; (5) excepting Mrm for morimotoite, symbols after [35].

In Ti-rich samples (Table 5), this method was found to be inappropriate and iron was assumed to be trivalent after the deduction of Fe^{2+} to compensate Ti, accepting the morimotoite substitution ($Fe^{2+}+Ti^{4+} \leftrightarrow 2Fe^{3+}$) rather than the schorlomite ($Si^{4+} \leftrightarrow Ti^{4+}$) one (e.g., [15,17]). The three generations of garnet identified at Măgureaua Vaţei have the main characteristics similar to those described at Cornet Hill [15].

Table 5. Representative compositions of Ti-rich garnets (grossular **II** and Ti-andradite), Măgureaua Vaței *.

Sample	2345	P8	2347	CE 5B	CE 5C	P6	PV2
Zone	A 1	B	B	BV	BV	C 1	C 2
N [(1)]	3	5	3	6	6	4	7
SiO_2	30.89	34.48	34.95	31.00	34.72	33.64	34.04
TiO_2	8.80	4.74	4.29	7.98	4.19	6.16	5.14
Al_2O_3	6.31	9.27	10.33	6.61	10.50	10.2	8.31
Cr_2O_3	-	-	-	0.11	0.05	-	-
Fe_2O_3 [(2)]	11.50	12.34	11.14	12.37	10.92	8.65	13.35
FeO [(2)]	7.91	4.26	3.86	6.78	3.6	5.54	4.62
MnO	0.03	0.07	0.02	0.04	0.09	0.08	0.04
MgO	0.64	0.57	0.34	0.69	0.66	0.68	0.52
CaO	34.10	34.77	35.06	33.90	34.78	34.73	34.57
Na_2O	0.01	0.02	0.02	0.01	0.00	0.00	0.02
K_2O	0.00	0.00	0.00	0.00	0.01	0.00	0.01
Total	100.19	100.52	100.01	99.49	99.52	99.68	100.62
Number of Cations on the Basis of 5 (Ca + Fe + Ti + Al + Cr + Mg + Mn + Na + K)							
Si	2.310	2.630	2.683	2.378	2.689	2.545	2.600
Ti	0.495	0.272	0.248	0.460	0.244	0.350	0.295
Al	0.556	0.833	0.935	0.598	0.958	0.910	0.748
Cr	-	-	-	0.006	0.003	-	-
Fe^{3+}	0.647	0.708	0.643	0.606	0.582	0.493	0.767
Fe^{2+}	0.495	0.272	0.248	0.460	0.244	0.350	0.295
Mn	0.002	0.005	0.001	0.002	0.005	0.005	0.003
Mg	0.071	0.065	0.039	0.079	0.077	0.077	0.059
Ca	2.732	2.842	2.883	2.786	2.886	2.815	2.829
Na	0.001	0.003	0.003	0.002	0.000	0.000	0.003
K	0.000	0.000	0.000	0.000	0.001	0.000	0.001
O	10.715	11.301	11.402	10.746	11.224	11.141	11.250
$(OH)^-$ [(3)]	2.570	1.398	1.196	2.508	1.552	1.718	1.500
$(OH)^-$ [(4)]	2.760	1.480	1.268	2.488	1.244	1.820	1.600
Composition in Terms of End-Members (mol.%) [(5)]							
Grs	32.70	45.85	51.13	35.75	53.47	51.81	41.25
Adr	38.10	39.05	35.21	36.29	32.57	28.12	42.38
Uv	-	-	-	0.36	0.17	-	-
Mrm	29.15	15.00	13.58	27.54	13.65	19.97	16.30
Prp	0.04	0.09	0.07	0.05	0.13	0.09	0.07
Sps	0.00	0.01	0.00	0.00	0.01	0.01	0.00

* Results expressed in wt.%; [(1)] number of point analyses; [(2)] as deduced from total iron (see text); [(3)] as deduced from the O^{2-} contents, for $[O + (OH)_2] = 12$ *apfu*; [(4)] as deduced from the Si contents, for $[Si + (OH)_4] = 3$ *apfu*; [(5)] excepting Mrm for morimotoite, symbols after [35].

A first generation of garnet (Table 4) consists in Ti-poor grossular, in fact a solid solution of grossular (53.51–81.03 mol.% Grs), andradite (43.63–16.74 mol.% Adr), minor morimotoite (up to 4.70 mol.%) and very minor "pyralspite" (0.18–0.82 mol.% Psp). This garnet generation (grossular **I**) was considered to be in equilibrium with gehlenite [4], and is generally restricted to the endoskarn zones and to BV gehlenite-bearing veins. Grossular **I** generally occurs as inclusions in gehlenite and rarely within the gehlenite crystals as atoll-disposed star-shaped crystals. Crystals of grossular **I** can include fine-grained patches of gehlenite + monticellite. With few exceptions, this grossular does not exhibit any intragranular compositional zoning and is sufficiently Si-depleted to assume (minor) hydrogarnet incorporation. Where zoned and develops "lamellar twinning", it may compositionally evolve by a slight enrichment in Fe^{2+} toward the rim. A second generation of garnet (sample 2347, CE 5C and P6 in Table 5) was encountered generally in outer endoskarn and inner

exoskarn zones. Equant crystals of this generation of garnet could also occur in the mass of wollastonite from the exoskarn, but are scarce. This generation (grossular **II**) is Ti-rich and always associates with gehlenite and wollastonite. The crystals are compositionally zoned, but the variations are quite modest; Ti and Fe are slightly enriched in the outer zones. The composition corresponds to a Fe- and Ti-rich grossular (51.13–53.47 mol.% Grs) with substantial andradite (35.21–28.12 mol.%) and morimotoite (13.58–19.97 mol.%). A third generation of garnet, (all but three analyses in Table 5), is an extremely coarse-grained titanian andradite that develops in subhedral to euhedral crystals as large as 2.5 cm in diameter, and generally displays a rimward increase in both andradite and morimotoite components, compensated by a slight decrease of the grossular content. It was described as "melanite" [5]. The mineral is black at macroscopic scale and reddish-brown in thin sections; it is apparently co-crystallized with wollastonite and its occurrence is restricted to the exoskarn zones. This garnet generation (garnet **III**) is isotropic and generally homogenous in composition. In some cases, composition within a single grain may vary, but no systematic zoning was observed. As well as at Cornet Hill [15], Ti-andradite appears to replace perovskite locally. The mean chemical compositions (Table 5) are indicative for Ti-andradite (36.29–42.38 mol.% Adr), with significant morimotoite (15.00–29.15 mol.% Mor) and grossular (32.70–45.85 mol.% Grs) components. The overall composition of each generation of garnet varies considerably, but not enough to change the general trend established on the basis of the data in Tables 4 and 5. The chemical variability of the calcic garnets from Măgureaua Vaţei is better depicted in Figure 6, where is compared with similar data on the garnets in the other two high-temperature skarn occurrences from Romania: Cornet Hill [15] and Oraviţa [17].

Representative cell parameters obtained for calcic garnets from Măgureaua Vaţei are given in Table 1. They clearly show the increase in a due to the incorporation of morimotoite, which is obvious in the case of Sample 2345.

The crystal structures of two calcic garnets whose chemistry is depicted in Table 5, i.e., a Ti-andradite (CE 5B) and a grossular **II** (CE 5C), were refined to 2.68% and 1.51% respectively, in the "classical" space group *Ia*3*d* (Table 2). The refined atomic coordinates and site occupancies, anisotropic displacement parameters and selected interatomic distances are available under request from the third author. The optical (sectorial) anomaly of birefringence observed in the case of CE 5C sample is then not due to a lowering of the symmetry of the garnet, but to a strain effect [9,10].

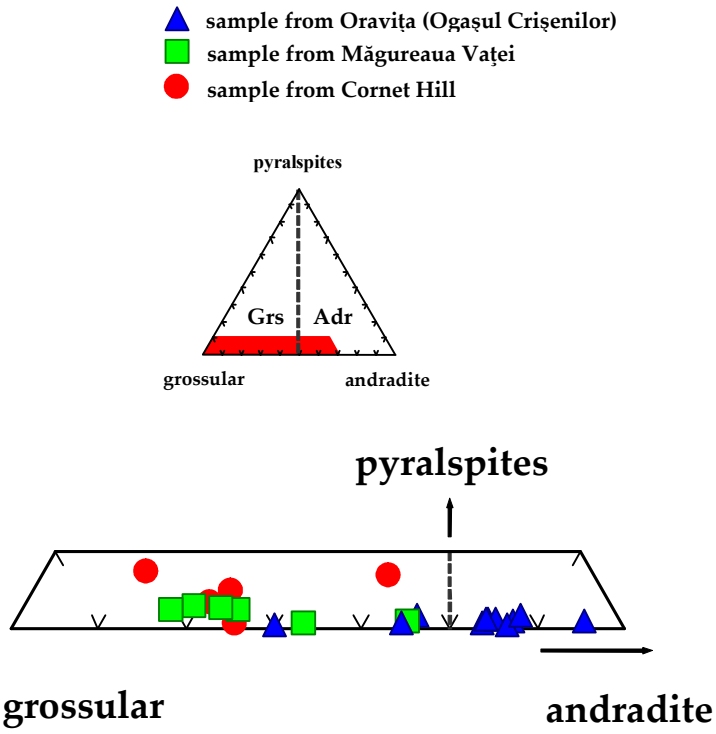

Figure 6. Ternary diagram showing the position of the calcic garnets in equilibrium with gehlenite in the grossular–andradite–pyralspites solid solution, particularized for the high-temperature skarns in Romania. Data from Cornet Hill as given by [15] and from Oraviţa as given by [17].

4.3. Diopside

Diopside is common in both the endoskarn and exoskarn zones from Măgureaua Vaţei. The mineral was identified in three textural contexts: (1) as disseminated crystals in a mass containing wollastonite in the endoskarn zones A1 and A2; on the outcrop from Crămuţ Valley, the crystals, of green color, may reach 3 mm in length; (2) rarely, as veins that transgress the gehlenite-bearing endoskarn in the B zone; and (3) as scarce, disseminated, and relatively small crystals (on average 0.4 mm × 0.1 mm) in the wollastonite mass or in Ti-andradite from the exoskarn zones (Figure 4C). In all cases, the mineral is quite close to the end-member diopside (Table 6). The calculation of chemical structural formulae assuming six cations of oxygen and all Fe as Fe^{3+} results in cation totals exceeding four, implying little, if any, Fe^{2+} is present the samples. Consequently, the "esseneitic" (ferri-Tschermak's) substitution in the octahedral M1 and M2 sites was accepted in the calculations of the formulas, which resulted in the compositions depicted in Table 6. In the innermost endoskarn zone (A1), diopside is Al-poor and Na-rich, whereas in the A2 and B zones, it generally contains significant esseneite and Ca-Tschermak components (Table 6). This pyroxene was described in more detail as "ferrian Ca-Tschermak pyroxene" [8]. The Ca-Tschermak substitution, as well as the Ca-Ti-Tschermak one, is significant in samples from the endoskarn, which parallels the findings of [8] for the clinopyroxenes from Măgureaua Vaţei (Table 6). The excess of calcium (Ca > 1 *apfu*) in all but one samples, imposes the calculation of a "wollastonite" component. This component is more important in a sample from the outer endoskarn (Table 6), and is not unexpected in clinopyroxene from high-temperature skarns: [39].

Table 6. Representative compositions of diopside, Măgureaua Vaţei *.

Sample	PV1	2346	P25 (3)	P34 (3)	2330 (3)	P1	P4	2347	2157
N (1)	3	4	5	4	4	3	3	3	3
Zone	A 1	A 2	A 2	A 2	A 2	B	B	B	C
SiO_2	52.27	41.84	50.69	50.08	51.05	53.55	42.10	54.99	50.36
TiO_2	0.51	0.81	0.29	0.31	0.34	0.14	0.54	0.07	0.24
Al_2O_3	1.29	14.60	4.80	6.40	4.46	1.87	15.22	0.38	5.76
FeO (2)	10.08	6.45	3.10	2.51	4.40	1.39	6.23	1.43	3.04
MnO	0.35	0.04	0.06	0.05	0.08	0.03	0.07	0.00	0.00
MgO	14.70	10.50	15.11	14.86	14.19	16.88	10.33	17.36	14.88
CaO	20.48	25.17	25.89	25.73	25.35	25.93	25.16	26.18	25.90
Na_2O	0.30	0.05	0.02	0.04	0.06	0.00	0.00	0.00	0.00
K_2O	0.00	0.00	0.01	0.00	0.01	0.01	0.00	0.00	0.01
Total	99.98	99.46	99.97	99.98	99.94	99.80	99.65	100.41	100.19
Number of Cations on the Basis of 6(O)									
Si	1.954	1.581	1.863	1.834	1.884	1.950	1.583	1.989	1.845
^{IV}Al	0.046	0.419	0.137	0.166	0.116	0.050	0.417	0.011	0.155
T sites	2.000	2.000	2.000	2.000	2.000	2.000	2.000	2.000	2.000
^{VI}Al	0.011	0.231	0.071	0.110	0.077	0.030	0.258	0.005	0.094
Ti	0.014	0.023	0.008	0.009	0.009	0.004	0.015	0.002	0.007
Fe^{2+}+ Fe^{3+}	0.315	0.204	0.095	0.077	0.136	0.042	0.196	0.043	0.093
Mn^{2+}	0.011	0.001	0.002	0.002	0.003	0.001	0.002	0.000	0.000
Mg	0.819	0.591	0.828	0.811	0.780	0.916	0.579	0.936	0.813
Ca	0.820	1.019	1.020	1.010	1.002	1.012	1.014	1.015	1.017
Na	0.022	0.004	0.001	0.003	0.004	0.000	0.000	0.000	0.000
K	0.000	0.000	0.000	0.000	0.000	0.000	0.000	0.000	0.000
M1+ M2 sites	2.014	2.073	2.026	2.021	2.012	2.006	2.064	2.001	2.024
Composition in End-Members (mol.%)									
diopside	71.53	69.27	86.09	86.54	82.03	93.66	69.35	94.67	85.72
hedenbergite	22.95	0.00	2.48	0.00	7.48	1.68	0.00	3.77	1.40
johansennite	1.07	0.08	0.18	0.18	0.27	0.10	0.15	0.00	0.00
aegirine	2.15	0.30	0.09	0.26	0.36	0.00	0.00	0.00	0.00
esseneite	2.30	18.80	6.73	7.32	5.62	2.48	17.99	0.55	7.54
Ca Tschermak	0.00	9.58	3.06	4.79	3.71	1.29	11.15	0.15	4.17
Ca-Ti Tschermak	0.00	1.06	0.39	0.43	0.43	0.20	0.69	0.10	0.34
"wollastonite"	0.00	0.91	0.98	0.48	0.10	0.60	0.66	0.75	0.83

* Results of electron-microprobe analyses, expressed in wt.%; (1) number of point analyses; (2) total iron expressed as FeO; (3) samples from Crămuţ Valley.

4.4. Wollastonite-2M

Wollastonite from the exoskarn zones from Cerboaia Valley has a spectacular development. In the C1 and particularly C2 zones, wollastonite occurs as almost mono-mineralic aggregates of long-prismatic or acicular crystals up to 10 cm in length. A microscopic view is offered in Figure 4B. In the endoskarn zones, as well as in the occurrence on Crămuţ Valley, a snow white wollastonite-rock, in which the mineral has abnormally low birefringence is composed of a compact aggregate of acicular or plumose to radiating prisms, having closely interlocking margins that show mosaic texture as observed at Carneal [40]. The size of crystals is very variable, the larger prisms reaching 1 cm in length. The mineral is commonly altered along fractures or in patches to very fine-grained material proven to be a mixture of tobermorite and okenite. A cathodo-luminescence zoning of some individual crystals could be observed on exposure to cold-cathode CL, and is illustrated in Figure 4D. As in the case of wollastonite sampled from Cornet Hill and Oraviţa, respectively [16,17], no solid evidence of correlation with the chemical zoning of the mineral was found, in spite of the evidence that one of the CL activators is the manganese.

The analyzed samples of wollastonite (Table 7) exhibit only relatively small deviations from the ideal composition: the substitutions of Ca in the six-fold coordinated sites (structure after Hesse

1984) are minor, with Mn < 0.004 *apfu*, Fe^{2+} < 0.107 *apfu* (generally much lower) and Mg < 0.043 *apfu* (on the basis of 18 oxygen atoms). In the formula from the table, all of the iron was allotted to the Ca site. The average composition of the analyzed grains is:

$(K_{0.002}Na_{0.004}Ca_{5.959}Mn_{0.004}Mg_{0.026}Fe^{2+}_{0.018})(Si_{5.984}Ti_{0.003}Al_{0.011})O_{18}$.

The density was measured for a selected sample (2292), using a Berman balance and toluene as displacement fluid, at 20 °C, is D_m = 2.90(1) g/cm^3. It compares favorably with the calculated density D_x = 2.915 g/cm^3, based on the chemical data in Table 7 and on cell parameters in Table 1, for Z = 12. The refraction indices measured for the same sample are α = 1.619(2), β = 1.632(2) and γ = 1.635(3). The mineral is optically negative, with 2V (measured) = 60°, which perfectly fits to the calculated value ($2V_{calc}$ = 50.99°).

The cell parameters of many samples are given in Table 1. In all cases, the diffraction effects were consistent with the monoclinic symmetry, space group $P2_1/a$. The obtained cell parameters (Table 1) are in good agreement with those given by [41] for the synthetic 2M polytype ("parawollsatonite"), i.e., a = 15.409(3) Å, b = 7.322(1) Å, c = 7.063(1) Å and β = 95.30(2)°.

The structural refinement of a representative sample of wollastonite was carried out in order to supplementary verify the polytypism, if existing. The refinement was successfully performed with a final agreement index R_1 = 0.0387, in the space group $P2_1/a$ (Table 2). Atomic positions and displacement parameters (U_{ij}) are given in Table 8, anisotropic temperature factors in Table 9, and bond lengths in Table 10, respectively. The resulted structure consists of chains of edge-sharing SiO_4 tetrahedrons, with a strong tendency to form Si_3O_9 ternary rings along the **c** axis, and octahedral layers of CaO_6 polyhedra. The general structure model proposed for parawollastonite [41] appears to be consistent.

Table 7. Representative electron-microprobe analyses of wollastonite, Măgureaua Vaţei *.

Sample	P25 (3)	P34 (3)	2530 (3)	2532 (3)	2554 (3)	2555 (3)	2297	P8	P5	CE 5B	2292	P6	PV2	2556
N (1)	3	3	10	11	15	11	8	4	3	5	11	4	3	11
Zone	A2	A2	A2	A2	A3	A3	A3	B	BV	BV	C1	C1	C2	C2
SiO_2	51.31	51.57	51.20	51.38	51.80	51.11	51.39	51.40	51.80	51.39	51.57	51.28	51.37	51.42
TiO_2	0.02	0.07	0.01	0.01	0.02	0.02	0.00	0.07	0.03	0.00	0.00	0.04	0.08	0.09
Al_2O_3	0.03	0.14	0.02	0.01	0.02	0.02	0.09	0.11	0.09	0.13	0.07	0.09	0.10	0.19
FeO (2)	1.10	0.09	0.12	0.16	0.19	0.10	0.09	0.10	0.15	0.12	0.11	0.14	0.03	0.09
MgO	0.21	0.10	0.14	0.20	0.14	0.17	0.11	0.15	0.25	0.12	0.14	0.12	0.12	0.16
MnO	0.09	0.00	0.04	0.06	0.05	0.03	0.07	0.05	0.00	0.02	0.06	0.05	0.01	0.04
CaO	47.23	47.97	47.88	47.93	47.71	47.78	47.72	48.01	47.64	47.52	47.84	48.26	48.05	47.64
Na_2O	0.01	0.01	0.01	0.01	0.01	0.01	0.01	0.05	0.02	0.00	0.01	0.02	0.10	0.00
K_2O	0.00	0.02	0.03	0.02	0.02	0.02	0.00	0.03	0.00	0.00	0.00	0.00	0.09	0.00
Total	100.00	99.97	99.45	99.78	99.96	99.26	99.48	99.97	99.98	99.30	99.80	100.00	99.95	99.63
Number of Cations on the Basis of 18 (O)														
Si	5.973	5.984	5.980	5.980	6.007	5.979	5.992	5.971	6.001	5.998	5.993	5.961	5.970	5.983
Ti	0.002	0.006	0.001	0.001	0.002	0.002	0.000	0.006	0.003	0.000	0.000	0.003	0.007	0.008
Al	0.004	0.019	0.003	0.001	0.003	0.003	0.012	0.015	0.012	0.018	0.010	0.012	0.014	0.026
Fe^{2+}	0.107	0.009	0.012	0.016	0.018	0.010	0.009	0.010	0.015	0.012	0.011	0.014	0.003	0.009
Mg	0.036	0.017	0.024	0.035	0.024	0.030	0.019	0.026	0.043	0.021	0.024	0.021	0.021	0.028
Mn	0.009	0.000	0.004	0.006	0.005	0.003	0.007	0.005	0.000	0.002	0.006	0.005	0.001	0.004
Ca	5.891	5.963	5.991	5.977	5.928	5.989	5.961	5.975	5.914	5.942	5.957	6.011	5.983	5.939
Na	0.002	0.002	0.002	0.002	0.002	0.002	0.002	0.011	0.004	0.000	0.002	0.005	0.023	0.000
K	0.000	0.003	0.004	0.003	0.003	0.003	0.000	0.004	0.000	0.000	0.000	0.000	0.013	0.000

* Results expressed in wt.%; (1) number of point analyses; (2) total iron as FeO; (3) samples from Crămuţ Valley.

Table 8. Atomic coordinates and isotropic equivalents (U_{eq}) in Å^2 for wollastonite (CE 5B).

Site	Atom	*x*	*y*	*z*	U_{eq}
Ca1	Ca	0.02741(7)	0.12485(11)	0.25169(3)	0.00838(13)
Ca2	Ca	0.26085(7)	−0.12797(9)	0.09933(3)	0.00889(13)
Ca3	Ca	0.26386(7)	0.37798(9)	0.10131(3)	0.00932(13)
Si4	Si	−0.44384(9)	0.12399(11)	0.19849(4)	0.00697(16)
Si5	Si	0.23097(10)	0.34124(10)	0.40751(5)	0.00727(17)
Si6	Si	0.23116(10)	−0.09208(10)	0.40761(5)	0.00703(17)
O	O	−0.3008(2)	0.1267(3)	0.28565(11)	0.0100(4)
O2	O	0.0350(3)	−0.1382(3)	0.34950(12)	0.0094(4)
O1	O	0.2337(3)	0.1239(3)	0.00880(12)	0.0133(4)
O4	O	0.2371(3)	−0.3697(3)	0.00947(12)	0.0129(4)
O2	O	0.3293(2)	0.1275(3)	0.20065(11)	0.0089(4)
O0	O	0.0364(2)	0.3846(3)	0.34793(12)	0.0104(4)
O5	O	0.5928(3)	−0.0551(3)	0.13626(12)	0.0115(4)
O3	O	0.5935(3)	0.3033(2)	0.13568(12)	0.0109(4)
O9	O	0.2748(3)	0.1248(3)	0.39113(12)	0.0131(4)

Table 9. Anisotropic temperature factors (Å^2) in wollastonite (CE 5B).

Site	U_{11}	U_{22}	U_{33}	U_{23}	U_{13}	U_{12}
Ca1	0.0089(2)	0.0074(3)	0.0089(3)	0.0001(2)	0.0015(2)	-0.0004(3)
Ca2	0.0096(3)	0.0077(3)	0.0095(3)	−0.0007(3)	0.0016(2)	−0.0009(3)
Ca3	0.0091(3)	0.0082(3)	0.0108(3)	0.0022(3).	0.0016(2)	0.0013(3)
Si4	0.0065(3)	0.0063(3)	0.0081(3)	0.0001(3)	0.0005(2)	−0.0002(3)
Si5	0.0072(3)	0.0072(4)	0.0075(3)	0.0000(3)	0.0008(2)	−0.0002(3)
Si6	0.0074(3)	0.0063(4)	0.0073(3)	−0.0002(3)	0.0005(2)	0.0007(3)
O	0.0083(9)	0.0122(9)	0.0094(9)	0.0043(9)	−0.0002(6)	0.0014(9)
O2	0.0088(9)	0.0094(9)	0.0097(9)	0.001(1)	0.0000(6)	0.001(1)
O1	0.018(1)	0.0124(9)	0.0089(9)	0.003(1)	0.0007(7)	0.009(1)
O4	0.019(1)	0.0112(9)	0.0081(9)	0.001(1)	0.0006(7)	0.007(1)
O2	0.0086(9)	0.0086(8)	0.0094(9)	−0.0004(9)	0.0009(6)	−0.0050(9)
O0	0.0082(9)	0.0125(9)	0.0103(9)	0.0036(10)	0.0001(6)	0.002(1)
O5	0.0093(9)	0.0105(9)	0.015(1)	−0.0020(7)	0.0010(7)	0.0016(8)
O3	0.0099(9)	0.0087(9)	0.014(1)	0.0026(7)	0.0011(7)	−0.0013(8)
O9	0.0155(9)	0.0068(8)	0.017(1)	0.0001(8)	0.0049(7)	−0.0008(9)

Table 10. Selected interatomic distances (Å) in wollastonite (CE 5B).

Ca(1)-O	2.426(2)	Ca(3)-O	2.518(2)	Si(5)-O(1)	1.581(2)
Ca(1)-O(2)	2.444(2)	Ca(3)-O(2)	2.314(2)	Si(5)-O(0)	1.612(2)
Ca(1)-O(2)	2.348(2)	Ca(3)-O(1)	2.342(2)	Si(5)-O(5)	1.656(2)
Ca(1)-O(2)	2.343(2)	Ca(3)-O(4)	2.325(2)	Si(5)-O(9)	1.639(2)
Ca(1)-O(0)	2.410(2)	Ca(3)-O(2)	2.407(2)	Mean Si(5)-O	1.622
Ca(1)-O(0)	2.351(2)	Ca(3)-O(3)	2.404(2)		
Ca(1)-O(9)	2.641(2)	Mean Ca(3)-O	2.385	Si(6)-O(2)	1.614(2)
Mean Ca(1)-O	2.423			Si(6)-O(4)	1.592(2)
		Si(4)-O	1.604(2)	Si(6)-O(3)	1.650(2)
Ca(2)-O	2.522(2)	Si(4)-O(2)	1.607(2)	Si(6)-O(9)	1.642(2)
Ca(2)-O(1)	2.310(2)	Si(4)-O(5)	1.660(2)	Mean Si(6)-O	1.624
Ca(2)-O(4)	2.244(2)	Si(4)-O(3)	1.667(2)		
Ca(2)-O(2)	2.456(2)	Mean Si(4)-O	1.634		
Ca(2)-O(0)	2.325(2)				
Ca(2)-O(5)	2.421(2)				
Mean Ca(2)-O	2.380				

4.5. Monticellite

Monticellite was first mentioned at Măgureaua Vaţei during previous investigations [4]. The mineral scarcely occurs in the gehlenite-bearing endoskarn (zone B), together with grossular **I** and a rankinite-like phase [4], as isolated crystals or as small veinlets interstitial to the gehlenite crystals. The individual crystals, with anhedral to subhedral contours, have up to 0.2 mm across (Figure 4A). The mineral is optical negative and shows a large optical angle ($-2V_\alpha$ = 80–80.5°) indicative for a magnesium-rich member of the monticellite–kirschsteinite series [42]. The indices of refraction measured for a representative sample of monticellite (sample P4) are α = 1.646(2), β (calculated for $2V_\alpha$ = 80°) = 1.653 and γ = 1.661(2). The measured density of the same sample is 3.13(1), which agrees well with the calculated density of 3.127 g/cm^3, based on the chemistry shown below and on the cell volume in Table 1.

The chemical composition of the mentioned sample is (in wt.% of oxides): SiO_2 = 37.08, TiO_2 = 0.05, CaO = 34.65, MgO = 21.39, MnO = 0.61, FeO = 5.98, Na_2O = 0.01, Total 99.77%. Normalized to 4 oxygen atoms, this yields to the formula:

$(Ca_{0.998}Na_{0.001})(Mg_{0.857}Fe^{2+}_{0.134}Mn_{0.018}Ti_{0.001})Si_{0.997}O_4$, which corresponds to a monticellite with only 13.28 mol.% kirschsteinite and 1.78 mol % glaucochroite in solid solution. Note that the index mg* = 100·Mg/(Mg + Fe + Mn) = 84.94, is under the values established for monticellite in skarns (mg* = 88.5–98.7: [43]), which is probably due to the higher iron content. On the other side, monticellite from Măgureaua Vaţei is Al-exempted, differing from this point of view from its Al-rich homologue from Oraviţa [17].

The cell parameters calculated for a representative sample are given in Table 1. They are larger compared with those calculated for a sample of monticellite with 9 mol.% kirschsteinite and 1 mol.% glaucochroite in solid solution, i.e., a = 4.821(2) Å, b = 11.105(3) Å and c = 6.381(1) Å [44], accounting for superior Fe^{2+}- and Mn-for-Mg replacements.

4.6. Vesuvianite

Vesuvianite typically occurs as euhedral crystals, with low birefringence, in the mass of wollastonite, but amoeboid rods engulfing gehlenite were also encountered. The mineral is clearly of primary origin in the first case, whereas in the second, it replaces gehlenite. Well-shaped, tetragonal- bipyramidal crystals of green vesuvianite up to 1 cm across occur in vacuoles of the wollastonite-2*M* mass in the C2 zone (Figure 3B).

Electron-microprobe traverses across crystals of both vesuvianite without reciprocal relationships with gehlenite and vesuvianite from replacement pods on gehlenite reveal a slight increase in Al/Fe from core to rim. Average compositions, taken as means of many randomly distributed point analyses within a crystal, are presented in Table 11. Boron was not measured. Vesuvianite formulae were normalized to 50 cations and 78 (O, OH, F, Cl) *pfu*, as recommended by [45]. Deviations from stoichiometry in vesuvianite, i.e., Si < 18 *apfu* of 50 cations and Ti + Al + Fe + Mg > 13 were recorded in all but two samples, and are characteristic of boron-bearing vesuvianite [45] or involve "hydrogarnet"-type substitutions.

The crystal structures of three vesuvianite samples, whose chemistry is depicted in Table 11, were refined in the "classical" space group *P*4/*nnc* (Table 2). The refined atomic coordinates and site occupancies, anisotropic displacement parameters and selected interatomic distances are available under request from the fifth author, and will be the subject of a further paper.

Table 11. Representative compositions of vesuvianite, Măgureaua Vaţei *.

Sample	P 34 (4)	2297	2303	2346	2347	CE 1A	P 6	PV 2	CE 2A	CE 8A
N (1)	4	4	4	4	4	4	2	3	3	3
Zone	A 2	A 3	B	B	B	B	C 1	C 2	C 2	C 2
SO_3	-	-	-	-	-	0.27	-	-	0.21	0.17
SiO_2	36.69	36.62	34.00	34.08	36.52	35.94	36.35	36.31	36.07	36.55
TiO_2	0.65	1.00	0.03	0.02	0.05	0.08	0.71	0.00	0.08	0.09
Al_2O_3	15.95	15.11	18.73	19.99	16.55	14.80	16.00	16.96	16.69	14.86
Cr_2O_3	-	-	-	-	-	0.01	-	-	0.00	0.03
CaO	36.51	36.62	37.84	38.19	37.64	35.54	36.44	37.51	36.09	36.26
MgO	4.18	3.13	3.63	4.05	4.49	4.27	4.12	4.10	3.52	4.65
MnO	0.05	0.03	0.06	0.03	0.02	0.14	0.02	0.07	0.03	0.17
FeO (2)	2.98	4.68	2.36	0.57	1.38	2.52	3.68	1.25	2.44	2.12
Na_2O	0.01	0.01	0.01	0.01	0.02	0.07	0.00	0.01	0.05	0.05
K_2O	0.01	0.01	0.01	0.00	0.00	0.01	0.00	0.03	0.00	0.01
F	0.01	0.01	0.02	0.06	0.10	0.68	0.02	0.01	0.37	0.53
Cl	0.00	0.00	0.01	0.28	0.04	0.13	0.01	0.00	0.03	0.09
H_2O (3)	3.48	3.43	3.97	3.90	3.63	3.36	3.58	3.55	3.27	3.48
	100.52	100.65	100.68	101.27	100.49	98.14	100.94	99.80	99.01	99.30
O = F,Cl	0.00	0.00	0.01	−0.09	−0.05	−0.32	−0.01	−0.00	−0.16	−0.24
Total	100.52	100.65	100.67	101.18	100.44	97.82	100.93	99.80	98.85	99.06
Number of Ions on the Basis of 50 Cations and 78 (O, OH, F, Cl)										
S^{6+}	-	-	-	-	-	0.101	-	-	0.077	0.062
Si	17.658	17.768	16.329	16.208	17.508	17.886	17.473	17.497	17.675	17.901
Ti	0.235	0.365	0.011	0.007	0.018	0.030	0.257	0.000	0.029	0.033
Al	9.047	8.640	10.602	11.205	9.351	8.680	9.064	9.632	9.639	8.577
Cr	-	-	-	-	-	0.004	-	-	0.000	0.012
Ca	18.826	19.036	19.471	19.460	19.334	18.950	18.767	19.366	18.948	19.027
Mg	2.999	2.264	2.599	2.871	3.209	3.168	2.952	2.945	2.571	3.395
Mn	0.020	0.012	0.024	0.012	0.008	0.059	0.008	0.029	0.012	0.071
Fe^{2+}	1.199	1.899	0.948	0.227	0.553	1.049	1.479	0.504	1.000	0.868
Na	0.009	0.009	0.009	0.009	0.019	0.068	0.000	0.009	0.048	0.047
K	0.006	0.006	0.006	0.000	0.000	0.006	0.000	0.018	0.000	0.006
F	0.015	0.015	0.030	0.090	0.152	1.070	0.030	0.015	0.573	0.821
Cl	0.000	0.000	0.008	0.226	0.032	0.110	0.008	0.000	0.025	0.075

$(OH)^-$	11.184	11.111	12.735	12.376	11.616	11.152	11.476	11.401	10.695	11.350

* Results of electron-microprobe analyses, expressed in wt.%; (1) number of point analyses; (2) total iron expressed as FeO; (3) as calculated for charge balance; (4) samples from Crămuţ Valley.

In all cases, the mineral is uniaxial negative and has low birefringence, sometimes in anomalous tints of Prussian blue, violet or brown (Figure 4E–G). An optical zoning, illustrated by Figure 4E–G, can be observed and could be correlated with the zonal variations of (Fe^{3+} + Ti) vs. Al ratios. Density determination on four separate clusters gave an average measured value of 3.35(2) g/cm^3. It compares well with the calculated densities in Table 2.

4.7. Hydroxylellestadite

An ellestadite-group mineral, identified as hydroxylellestadite or rather as a Si- and S-bearing hydroxylapatite, occurs as scattered at random oriented grains throughout the gehlenite mass. The mineral has euhedral to subhedral, equant to short prismatic habit. Grains have an average diameter of 0.1 mm, with a maximum length of about 0.2 mm. No chemical or optical zoning was observed. A thin overgrowth of thaumasite surrounds some of the crystals. The average chemical analysis obtained as result of six point-analyses performed by EMPA on three different crystals of hydroxylellestadite from a gehlenite-, garnet-, monticellite- and vesuvianite-bearing sample is (in wt.% of oxides): SO_3 = 9.94, P_2O_5 = 22.23, SiO_2 = 9.64, TiO_2 = 0.02, CaO = 55.37, FeO = 0.03, Na_2O = 0.03, K_2O = 0.01, F = 0.86, Cl = 0.59, H_2O (as calculated for charge balance) = 0.77, (F,Cl) = O = 0.50, Total = 98.99. Normalized to 3 (P + Si + S) and 13(O,OH,F,Cl) *pfu*, this yields to the formula:

$Ca_{4.955}Fe_{0.002}Ti_{0.001}Na_{0.005}K_{0.001}(Si_{0.805}P_{1.572}S_{0.623})[O_{12.000}(OH)_{0.431}F_{0.227}Cl_{0.084}]$.

4.8. H_4O_4-Substituted Grossular ("Hibschite")

EMP analyses of some isotropic coatings of gehlenite crystals with distinct garnet habit or on spots of "patched gehlenite" [4] revealed Si deficits and low totals as referred on "normal" garnet compositions, than the presence of a hydrogarnet. The most representative hydrogarnet compositions were obtained from specimens found as isotropic fringes of 20 μm–0.1 mm thick developed on gehlenite crystals or interstitial to vesuvianite ones (Figure 4G). The refraction indices measured on these fringes are of 1.64–1.65, being identical to these reported for samples from Carneal (Northern Ireland): [40].

The chemical composition of a representative sample (sample 2303), is given in Table 12. All iron was considered in trivalent state of oxidation. The chemical-structural formula corresponding to this composition is:

$(Ca_{2.868}Mn_{0.004}Mg_{0.372})(Al_{1.658}Fe^{3+}_{0.096}Ti_{0.002})(SiO_4)_{2.395}(OH)_{2.175}Cl_{0.003}$.

This formula fairly approximates the "hibschite" ideal formula $Ca_3Al_2(SiO_4)_{3-x}(OH)_{4x}$, with x < 1.5 [46].

The cell parameters of two "hibschite" samples from Măgureaua Vaţei are given in Table 1. Both of them are smaller than the similar parameter calculated for "hibschite" in the high-temperature skarn from the nearby occurrence, Cornet Hill, i.e., *a* = 11,982(2) Å [15], suggesting lower contents of the $Ca_3Al_2(OH)_{12}$ component.

Table 12. Representative compositions of selected secondary minerals in the Măgureaua Vaţei skarns *.

Sample	**2303**	**2303**	**2303**	**1519**
N (1)	5	5	5	6
Mineral	"hibschite"	clinochlore	lizardite	dickite
SiO_2	32.63	36.79	39.52	41.39
TiO_2	0.04	0.01	0.03	0.03
Al_2O_3	19.17	13.00	4.94	32.13
Fe_2O_3 (2)	1.73	-	-	1.47
FeO (2)	-	1.49	0.62	-
CaO	36.47	0.80	0.09	1.00
MgO	3.40	34.82	37.88	4.50
MnO	0.06	0.19	0.29	-
Na_2O	-	-	-	0.08
K_2O	-	0.03	-	0.17

Cl	0.02	0.01	-	0.01
H_2O (3)	5.43	12.18	12.43	12.78
	98.95	99.31	-	93.56
O=Cl	−0.005	−0.002	-	−0.002
Total	98.945	99.308	95.80	93.558
Formulae on the Basis of X Ions (4)				
Si	2.395	6.920	3.812	3.882
^{IV}Al	-	1.080	0.188	0.118
Ti	0.002	0.001	0.002	0.002
^{VI}Al	1.658	1.802	0.374	3.434
Fe^{3+}	0.096	-	-	0.104
Fe^{2+}	-	0.234	0.050	-
Ca	2.868	0.161	0.009	0.101
Mg	0.372	9.764	5.446	0.629
Mn	0.004	0.031	0.024	-
Na	-	-	-	0.016
K	-	0.007	-	0.020
Cl	0.003	0.003	-	0.002
$(OH)^-$	2.659	15.282	8.000	7.998
O^{2-}	9.338	20.715	10.000	10.000

* Results of electron-microprobe analyses, expressed in wt.%; (1) number of point analyses; (2) total iron expressed as Fe_2O_3 in "hibschite" and dickite and as FeO in clinochlore and lizardite; (3) as calculated for charge balance; (4) X = 5 (Ca + Mg + Mn + Al + Fe^{3+} + Ti) and 12 (O, OH, Cl) *pfu* for "hibschite", 20 cations and 36 (O, OH, Cl) *pfu* for clinochlore, 10(O) + 8(OH, Cl) *pfu* for lizardite and dickite.

4.9. Clinochlore

Clinochlore scarcely occurs in the endoskarn zone from Măgureaua Vaţei (Cerboaia Valley) [4]. The mineral occurs as isolated pseudo-hexagonal platy crystals up to 0.2 mm across, associated with serpentine and engulfed by the vesuvianite mass. Microscopically, the mineral is optically positive and has low but not anomalous birefringence. The X-ray diffraction on carefully hand-picked separates shows that the analyzed chlorite is tri-octahedral [47], since the (003) "basal" reflection at about 4.7 Å has small intensities as compared with the even (002) and (004) reflections. The six-fold coordinated iron, estimated on the basis of the graphical method recommended by [48], on the basis of the $I_{(002)}/I_{(004)}$ ratio, is ~0.22 *apfu*. This suggests that the Fe/(Fe + Mg) ratio will be most probably smaller than 0.2, which is characteristic for clinochlore [48].

The cell parameters obtained for one representative sample are given in Table 1, whereas a chemical analysis is reported in Table 12. The analysis was normalized on the basis of 20 cations and 36 (O, OH, F, Cl) *pfu* [49]. All iron was assumed to be in divalent state of oxidation, after the optimization of the ideal occupancy of the six-fold coordination sites on the basis of charge balance. The chemical-structural formula, calculated on the basis of 20 cations and 36 (O,OH,Cl) *pfu* [49] is given in Table 12. The values of the indices x = Fe^{2+} + Fe^{3+} (*apfu*) and R = (Fe^{2+} + Fe^{3+})/(Fe^{2+} + Fe^{3+} + Mg) are x = 0.234 and R = 0.023, respectively; these values are characteristic for clinochlore ("pennine" according to the Hey's, diagram: [50]), in perfect agreement with the diffraction data.

4.10. Chrysotile and Lizardite

Serpentine group minerals were first identified as fine-grained infillings of fractures affecting vesuvianite replacing gehlenite in the endoskarn, as well as infilling of very fine interstitial spacings between wollastonite and grossular **I** replacing diopside in the A1 zone [4]. These minerals were retrieved as thin borders, up to 0.02 mm thick, of vesuvianite relics, as well as in "mesh textures" that probably represent pseudomorphs on monticellite. They always have low birefringence, positive elongation and are optically negative, behaving like a γ-serpentine [51]. Isotropic nuclei suggest the presence of associated lizardite. Taking into account the identity between γ-serpentine and chrysotile [51] we suppose that the serpentine group mineral from Măgureaua Vaţei is

chrysotile. The XRD study of a heavy liquid separate with D < 2.65 g/cm^3 proved the presence of a high intensity reflection centered at 2.494–2.504 Å, as well as the lack of the "antigorite" reflection at ~1.563 Å and the presence of the lizardite "doublet" at ~1.502 and ~1.535 Å respectively, which accounts for the occurrence, at Măgureaua Vaţei, of a chrysotile + lizardite mixture (cf., [52]).

A chemical analysis of a selected sample of serpentine is given in Table 12, as well as the chemical-structural formula calculated on the basis of 10(O) + 8(OH) *pfu*. The analysis fits with the lizardite composition [53], since: (1) the tetrahedral positions are fully occupied, with a substantial Al occupancy; (2) the sum of six-fold coordinated cations (5.905 *apfu*) is close to the ideal value of 6 *apfu*, and in the range of the values given for lizardite (5.91–6.04 *apfu*: [53]); (3) the Si/Mg ratio is of 1.04, very close to that in the stoichiometris serpentine (Si/Mg = 1.01); (4) the calculation of formula on a cationic base (excepting H) indicates an excess of positive charges, which are due to the excess of water, as compared with the stoichiometric serpentine.

4.11. Dickite

Dickite occurs as tinny plates up to 50 μm across in the white-yellow earthy crusts that overcoat gehlenite crystals in the outcrop at the Upper Cerboaia Valley. These crusts probably represent a product of weathering [5]. The mean index of refraction of this material is n = 1.56. The XRD study reveals the presence of a "7-Á layered structure" that reacts by splitting the (001) spacing at 7.06 Á after saturation with hydrazine. This phase can be then positively identified as a mineral from the kaolinite group instead a chlorite [54], [55]. The cell parameters were calculated on the basis of the X-ray powder diffraction pattern of a separate (sample 1509), using both the triclinic (space group *P*1) and monoclinic (space group *Cc*) indexing. The best fitting was obtained for a monoclinic cell having the parameters in Table 1, that are, however, different in detail from those given for dickite, i.e., a = 5.1474(6) Å, b = 8.9386(10) Å, c = 14.390(2) Å, and β = 96.483(1)° [56]. The presence at Măgureaua Vaţei of a mixture of dickite and kaolinite is not excluded. The chemical composition of dickite is given in Table 12. The low total after the calculation of water for charge balance indicates a high degree of hydration of the sample. The density of the sample, as calculated from the chemical composition and the cell volume, assuming Z = 2 formula units per unit cell [56], is D_x = 2.677 g/cm^3. This value is higher than that measured in by sink float in a mixture of bromoform and toluene [D = 2.64(1) g/cm^3].

4.12. Okenite

Okenite generally occurs in veins and as fibrous aggregates either within wollastonite grains or cutting across wollastonite–gehlenite grain boundaries. A closer view shows that the mineral is present in discrete radiating aggregates, some of these being associated with very narrow veinlets and aggregates of calcite and tobermorite (Figure 4H). Although these veins are generally monomineralic, veining by mixed tobermorite and okenite may be present, as observed at Carneal [40] in the case of xonotlite + tobermorite association.

The unit cell data obtained for a selected sample of okenite (CE 8) by least-squares refinement of the XRD data are: a = 9.71(2) Å, b = 7.22(l) Å, c = 21.59(7) Å, α = 91.3(2)°, β = 101.7(5)°, γ = 111.8(4)°. They fit well with those given for a sample from Kolhapur (India): a = 9.69(l) Å, b = 7.28(l) Å, c = 22.02(4) Å, α = 92.7(2)°, β = 100.1(3)°, γ = 110.9(l)°: [57].

4.13. Calcite

Secondary, residual or recrystallized calcite occurs frequently on the fissures affecting the wollastonite mass, and is interstitial to fills fractures or penetrates on an extremely fine scale along the cleavages and crystal boundaries of the wollastonite crystals. As a characteristic feature, the remobilized (interstitial) calcite has a bluish tint, whereas the secondary calcite, issued in most of the cases from the recrystallization of aragonite or of CSH gels, occurs as white, fibrous or earthy masses. The chemical compositions of the two calcite types differ in detail. A mean composition of the remobilized calcite, taken as mean result of ten point analyses on different crystals, is (in wt.%):

CaO = 55.94, MgO = 0.04, MnO = 0.03, FeO = 0.02, CO_2 (as calculated for stoichiometry) = 43.97. The chemical composition of the secondary calcite, measured on 6 calcite rims on wollastonite or on calcite penetrating fractures in wollastonite crystals is (in wt.%): CaO = 55.89, MgO = 0.09, MnO = 0.04, CO_2 = 43.98. The chemical-structural formulas deduced from the mean compositions given before are $Ca_{1.996}Mg_{0.002}Mn_{0.001}Fe^{2+}_{0.001}(CO_3)_2$ and $Ca_{1.995}Mg_{0.004}Mn_{0.001}(CO_3)_2$, respectively, being in both cases close to the calcite end-member.

The unit-cell parameters of three representative samples are given in Table 1. Note that Sample 2530 is of remobilized calcite, whereas the other two samples are of secondary origin, lining wollastonite crystals. In all cases, the cell parameters are close to those refined for the stoichiometric calcite [a = 4.9896(2) Å and c 17.0610(11) Å]: [58], which fit with the chemical analyses.

4.14. Tobermorite

As well as in the similar occurrence from Cornet Hill [15], a 11-Å phase, identified as tobermorite, was identified on the XRD patterns. This phase most commonly occurs as bunches, sheaf-like or radiating aggregates of acicular or fibrous crystals up to 30 μm long and 1 μm wide intergrown with okenite (Figure 2F). It is similar in habit to the tobermorite from Ballycraigy (Northern Ireland): [59]. The spatial relationship between okenite and tobermorite suggests that okenite preceded tobermorite. Fibers of tobermorite are too small to permit a good optical characterization. The mean index of refraction is 1.553(5), which compares favorably with that measured for tobermorite from the "Mottled Zone" complex, Israel ($\overline{n}$ = β = 1.552): [60]. No reliable EMP analyses were obtained, due to the very fine-grained nature of the mineral.

4.15. Allophane (SHA or CSHA Gels)

Among the weathering phases, there are poorly crystalline pods of hydrogarnet + allophane replacing gehlenite. EMP analyses of ten pods with porous or gel-like appearance show that they contain only Al and Si or, in three cases, Ca, Al and Si as main elements. These are very fine-grained, X-ray amorphous, and can also associate with aragonite, calcite, tobermorite and okenite. This kind of association is particularly visible along fractures, cracks and veinlets that cross-cut the gehlenite mass. A broad hump centered at 3.29–3.41 Å on the XRD patterns is consistent with the presence of allophane [61]. The material has a mean index of refraction that varies from sample to sample between 1.470 and 1.485, possibly because of variable degree of hydration.

5. Discussion

As well as in other occurrences of high-temperature skarns from Romania (e.g., [15,17]) the association of skarn minerals from Măgureaua Vaţei could be imagined as a succession of metamorphic events, resulting in overprinting parageneses. The data presented before support previous interpretations, as follows:

(1) A first metamorphic (metasomatic) event is prograde. The maximum temperature conditions estimated for this M1 event of prograde evolution of the system are in the range of 760–800 °C, at pressures of up to 0.5 kbar [8]. The peak metamorphic assemblage contains gehlenite, diopside (with substantial content of Ca-Tschermak molecule), wollastonite-2*M* and monticellite. The peak temperatures agree with those estimated by us, taking into account the experimental data published [62,63]; according these data, gehlenite is stable between 800 °C and at 827 °C, at pressures of carbon dioxide ranging from 100 to 200 bar. The presence of wollastonite in the external zones imposes an activity (α) of SiO_2 in the fluid greater than 10^{-2} and a high activity of CO_2, which explains the absence of carbonate-bearing silicates such as tilleyite and spurrite. On the other side, the abundance of gehlenite in the inner skarn zones implies that the activity of Al_2O_3 in the fluid is lower than 10^{-1}.

(2) A second event (M2) coincides with the crystallization of vesuvianite, "hibschite", hydroxylellestadite, clinochlore and is essentially retrogressive and hydrothermal. This moment corresponds to the recrystallization of calcite in excess, to form calcite I. This event was oxidizing,

as evidenced, respectively, by the relatively high Fe^{3+} contents of vesuvianite, by the high Fe^{3+}/Fe value in clintonite and by the presence of hydroxylellestadite. The peak temperatures are estimated at up to 600 °C, this event ending at temperatures of about 350 °C.

(3) A later hydrothermal event (M3) is clearly retrogressive and induces the formation of lizardite, chrysotile, dickite, thaumasite, okenite and tobermorite, as products of retrogressive alteration of the pre-existing phases. Weathering overprints all the previous assemblages. Within the weathering paragenesis, the most common supergene silicate is okenite (which essentially replaces wollastonite, but also vesuvianite and "hibschite") and allophane (which alters both primary phases e.g., gehlenite, vesuvianite and secondary ones e.g., "hibschite", tobermorite and okenite).

Supplementary Materials: The following are available online at www.mdpi.com/xxx/s1, Table S1. X-ray powder data of selected samples of gehlenite from Măgureaua Vaţei (Cerboaia Valley); Table S2. X-ray powder data for selected samples of grossular **I** from Măgureaua Vaţei; Table S3. X-ray powder data for selected samples of titanian garnet from Măgureaua Vaţei; Table S4. X-ray powder data for a representative sample of monticellite from Măgureaua Vaţei (Sample P4, Cerboaia Valley); Table S5. X-ray powder data for selected samples of vesuvianite from Măgureaua Vaţei (Cerboaia Valley); Table S6. X-ray powder data for selected samples of "hibschite" (H_4O_4-substituted grossular) from Măgureaua Vaţei; Table S7. X-ray powder data for selected samples of secondary calcite from Măgureaua Vaţei; Table S8. X-ray powder data for selected samples of kaolinite from Măgureaua Vaţei (sample 1519).

Author Contributions: Conceptualization, S.M., D.-G.D. and F.H.; formal analysis, S.M., C.S., F.D.B.; funding acquisition, S.M. and F.H.; investigation, S.M., D.-G.D., C.S., F.H. and F.D.B.; methodology, S.M., D.-G. D., F.H. and F.D.B.; resources, S.M., D.-G.D. and F.H.; data curation, D.-G.D., C.S., F.H. and F.D.B.; writing—original draft preparation, S.M.; writing—review and editing, S.M.; visualization, S.M.; supervision, S.M.; project administration, S.M., C.S. and F.H. All authors have read and agreed to the published version of the manuscript.

Funding: This study was partly supported by a scientific research grant awarded to the first author by the Walloon Government (Belgium) in 2011 (AMG/VDL/Ide/IN WBI/SOR/2011/8499). Other grants allowed to the first author by UEFISCDI in Romania (PN-II-ID-PCE-2011-3-0023, PN-III-P1-1.2-PCCDI-2017-0346 and PN-III-P1-1.1-MC-2018-3163) generously supported the final draft. C.S. gratefully acknowledges the receipt of a UEFISCDI grant (PN-III-P1-1.1-MC-2018-3199) which helped to obtain part of the structure refinements.

Acknowledgments: Régis Piret (Université Catholique de Louvain, Belgium) and Gelu Costin (Rice University, Houston, U.S.) kindly communicated some of the XRD and EMP analyses used for this study. Many other primary data were kindly provided by Julie Vanheyste, and some of the photos used to illustrate the textural relations between minerals were offered by Denis Cavenaile, both of them from Université de Liège. Fruitful discussions in the field with the lates Jean Verkaeren and Avram Ştefan, with Gheorghe Ilinca, Jacqueline Vander Auwera, Marie Lola Pascal, Ildiko Katona, André-Mathieu Fransolet, Maxime Baijot, Evgheny Galuskin, Irina Galuskina and Robert Martin are highly appreciated.

Conflicts of Interest: The authors declare no conflict of interest.

References

1. Grapes, R. *Pyrometamorphism*, 2nd ed.; Springer: Berlin/Heidelberg, Germany, 2010; pp. 1–364.
2. Reverdatto, V.V. *The Facies of Contact Metamorphism*; Sobolev, V.S., Ed.; Nedra: Moscow, Russia, 1970; pp. 1–263. (In Russian).
3. Piret, R. Minéralogie et Géochimie des Skarns de Haute Température des Régions de Măgureaua Vaţei et de Cornet Hill (Monts Apuseni). Master's Thesis, Université Catholique de Louvain, Louvain-la-Neuve, Belgium, 1997.
4. Pascal, M.-L.; Fonteilles, M.; Verkaeren, J.; Piret, R.; Marincea, Ş. The melilite-bearing high-temperature skarns of the Apuseni Mountains, Carpathians, Romania. *Can. Mineral*. **2001**, *39*, 1405–1434.
5. Ştefan, A.; Istrate, G.; Medeşan, A. Gehlenite in calc-skarns from the Măgureaua Vaţei—Cerboaia (Apuseni Mountains—Romania). *Rev. Roum. Géol. Géophys. Géogr. Sér. Géol*. **1978**, *22*, 155–160.
6. Marincea, Ş.; Dumitraş, D.G.; Ghineţ, C.; Fransolet, A.-M.; Hatert, F.; Rondeux, M. Gehlenite from three occurrences of high-temperature skarns, Romania: New mineralogical data. *Can. Mineral*. **2011**, *49*, 1001–1014.

7. Marincea, Ş.; Dumitraş, D.G. Monticellite and hydroxylellestadite in high-temperature skarns from Romania. *Acta Mineral.-Petrogr. Abstr. Ser.* **2003**, *1*, 68.
8. Pascal, M.-L.; Katona, I.; Fonteilles, M.; Verkaeren, J. Relics of high-temperature clinopyroxene on the join Di-CaTs with up to 72 mol.% Ca(Al, Fe^{3+})$AlSiO_6$ in the skarns of Ciclova and Măgureaua Vaţei, Carpathians, Romania. *Can. Mineral.* **2005**, *43*, 857–881.
9. Takéuchi, Y.; Haga, N.; Umizu, S.; Sato, G. The derivative structure of silicate garnets in grandite. *Z. Kristallogr*. **1982**, *158*, 53–99.
10. Shtukenberg, A.G.; Punin, Y.O.; Frank-Kamenetskaya, O.V.; Kovalev, O.G.; Sokolov, P.B. On the origin of anomalous birefringence in grandite garnets. *Mineral. Mag.* **2001**, *65*, 445–459.
11. Krivovichev, S.V.; Yakovenchuk, V.N.; Panikorovskii, T.L.; Savchenko, E.E.; Pakhomovsky, Y.A.; Mikhailova, Y.A.; Selivanova, E.A.; Kadyrova, G.I.; Ivanyuk, G.Y. Nikmelnikovite, $Ca_{12}Fe^{2+}Fe^{3+}3Al_3(SiO_4)_6(OH)_{20}$, a new mineral from Kovdor massif (Kola peninsula, Russia). *Dokl. Earth Sci.* **2019**, *488*, 1200–1202.
12. Henmi, C.; Kawahara, A.; Henmi, K.; Kusachi, I.; Takéuchi, Y. The 3*T*, 4*T* and 5*T* polytypes of wollastonite from Kushiro, Hiroshima Prefecture, Japan. *Am. Mineral.* **1983**, *68*, 156–163.
13. Gnos, E.; Armbruster, T. Relationship among metamorphic grade, vesuvianite "rod polytypism", and vesuvianite composition. *Am. Mineral.* **2006**, *91*, 862–870.
14. Ohkawa, M.; Armbruster, T.; Galuskin, E. Structural investigation of low-symmetry vesuvianite collected from Tojyo, Hiroshima, Japan: Implications for hydrogarnet-like substitutions. *J. Mineral. Petrol. Sci.* **2009**, *104*, 69–76.
15. Marincea, Ş.; Bilal, E.; Verkaeren, J.; Pascal, M.L.; Fonteilles, M. Superposed parageneses in the spurrite-, tilleyite-, and gehlenite-bearing skarns from Cornet Hill, Apuseni Mountains, Romania. *Can. Mineral*. **2001**, *39*, 1435–1453.
16. Marincea, Ş.; Dumitraş, D.G.; Călin, N.; Anason, A.M.; Fransolet, A.-M.; Hatert, F. Spurrite, tilleyite and associated minerals in the exoskarn zone from Cornet Hill (Metaliferi Massif, Apuseni Mountains, Romania). *Can. Mineral*. **2013**, *51*, 359–375.
17. Marincea, Ş.; Dumitraş, D.G.; Ghineţ, C.; Bilal, E. The occurrence of high-temperature skarns from Oraviţa (Banat, Romania): A mineralogical overview. *Can. Mineral*. **2015**, *53*, 511–532.
18. Cioflica, G.; Vlad, Ş. The correlation of the Laramian metallogenetic events belonging to the Carpatho-Balkan area. *Rev. Roum. Géol. Géophys. Géogr. Sér. Géol.* **1973**, *17*, 217–224.
19. Săndulescu, M.; Kräutner, H.; Borcoş, M.; Năstăseanu, S.; Patrulius, D.; Ştefănescu, M.; Ghenea, C.; Lupu, M.; Savu, H.; Bercia, I.; et al. *Geological Map of Romania, Scale 1:1,000,000*; Institute of Geology and Geophysics: Bucharest, Romania, 1978.
20. Berza, T.; Constantinescu, E.; Vlad, Ş.N. Upper Cretaceous magmatic series and associated mineralizations in the Carpathian-Balkan orogen. *Res. Geol.* **1998**, *48*, 291–306.
21. Ciobanu, C.L.; Cook, N.J.; Stein, H. Regional setting and geochronology of the Late Cretaceous Banatitic Magmatic and Metallogenetic Belt. *Miner. Depos.* **2002**, *37*, 541–567.
22. Zimmermann, A.; Stein, H.; Hannah, J.; Koželj., D.; Bogdanov, K.; Berza, T. Tectonic configuration of the Apuseni-Banat-Timok-Srednogorie belt, Balkans-Southern Carpathians, constrained by high precision Re-Os molybdenite ages. *Miner. Depos.* **2008**, *43*, 1–21.
23. Ştefan, A.; Lazăr, C.; Berbeleac, I.; Udubaşa, G. Evolution of the Banatitic magmatism in the Apuseni Mts. and the associated metallogenesis. *D. S. Inst. Geol. Geofiz.* **1988**, *72*, 195–213.
24. Săbău, G.; Negulescu, E. Peritectic metasomatism and agpaitic line of descent in the endocontact zone of the Măgureaua Vaţei (MV) intrusives (Apuseni Mts.). In Proceedings of the V. M. Goldschmidt Conference 2014, Sacramento, Program and Abstracts, Sacramento, CA, USA, 8–13 June 2014; Volume 24, p. 2155.
25. Ştefan, A.; Roşu, E.; Andăr, A.; Robu, L.; Robu, N.; Bratosin, I.; Grabari, G.; Stoian, M.; Vâjdea, E.; Colios, E. Petrological and geochemical features of banatitic magmatites in Northern Apuseni Mountains. *Rom. J. Petrol*. **1992**, *75*, 97–110.
26. Bleahu, M.; Soroiu, M.; Catilina, R. On the Cretaceous tectonic–magmatic evolution of the Apuseni Mountains as revealed by K–Ar dating. *Rev. Roum. Phys.* **1984**, *29*, 123–130.
27. Lupu, M.; Avram, E.; Antonescu, E.; Dumitrică, P.; Lupu, D.; Nicolae, I. The Neojurassic and the Cretaceous of the Drocea Mts.: The stratigraphy and the structure of an ensialic marginal basin. *Rom. J. Tecton. Reg. Geol.* **1993**, *75*, 53–66.

28. Pouchou, J.L.; Pichoir, F. PAP ϕ (ρZ) procedure for improved quantitative microanalysis. In *Microbeam Analysis*; Armstrong, J.T., Ed.; San Francisco Press: San Francisco, CA, USA, 1985; pp. 104–106.
29. Appleman, D.E.; Evans, H.T., Jr. Indexing and least-squares refinement of powder diffraction data. *US Geol. Surv. Comput. Contrib.* **1973**, *20*, 60.
30. Benoit, P.H. Adaptation to microcomputer of the Appleman-Evans program for indexing and least-squares refinement of powder-diffraction data for unit-cell dimensions. *Am. Mineral.* **1987**, *72*, 1018–1019.
31. Agilent Technologies. *Xcalibur CCD System, CrysAlis Software System*; Agilent Technologies: Yarnton, Oxfordshire, UK, 2012.
32. Sheldrick, G.M. A short history of SHELX. *Acta Crystallogr.* **2008**, *A64*, 112–122.
33. Dolomanov, O.V.; Bourhis, L.J.; Gildea, R.J.; Howard, J.A.K.; Puschmann, H. OLEX2: A complete structure solution, refinement and analysis program. *J. Appl. Cryst.* **2009**, *42*, 339–341.
34. Strunz, H.; Nickel, E.H. *Strunz Mineralogical Tables, Collection*, 9th ed.; Schweizerbart'sche Verlangsbuchhandlung: Berlin/Stuttgart, Germany, 2001; pp. 1–870.
35. Whitney, D.L.; Evans, B.W. Abbreviations for names of rock-forming minerals. *Am. Mineral.* **2010**, *95*, 185–187.
36. Louisnathan, S.J. Refinement of the crystal structure of a natural gehlenite, $Ca_2Al(Al,Si)_2O_7$. *Can. Mineral.* **1971**, *10*, 822–837.
37. Armbruster, T.; Birrer, J.; Libowitzky, E.; Beran, A. Crystal chemistry of Ti-bearing andradites. *Eur. J. Mineral.* **1998**, *10*, 907–921.
38. Droop, G.T.R. A general equation for estimating Fe^{3+} concentrations in ferromagnesian silicates and oxides from microprobe analyses, using stoichiometric criteria. *Mineral. Mag.* **1987**, *51*, 431–435.
39. Tilley, C.E. The zoned contact-skarns of the Broadford area, Skye: A study of boron-fluorine metasomatism in dolomites. *Mineral. Mag.* **1951**, *29*, 622–666.
40. Sabine, P.A.; Young, B.R. Metamorphic processes at high temperature and low pressure: The petrogenesis of the metasomatized and assimilated rocks of Carneal, Co. Antrim. *Phil. Trans. R. Soc. Lond.* **1975**, *280*, 225–269.
41. Hesse, K.-F. Refinement of the crystal structure of wollastonite-2*M* (parawollastonite). *Z. Kristall.* **1984**, *168*, 93–98.
42. Nikishov, K..; Nikishova, L.V. The possibility of reaction between olivine and monticellite. *Geochem. Int.* **1966**, *3*, 1200–1206.
43. Deer, W.A.; Howie, R.A.; Zussman, J. *Rock-Forming Minerals 1A Orthosilicates*, 2nd ed.; Longman Ed.: London, UK; New York, NY, USA, 1982; pp. 1–919.
44. Sharp, Z.D.; Hazen, R.M.; Finger, L.W. High-pressure crystal chemistry of monticellite, $CaMgSiO_4$. *Am. Mineral.* **1987**, *72*, 748–755.
45. Groat, L.A.; Hawthorne, F.C.; Ercitt, T.S. The chemistry of vesuvianite. *Can. Mineral.* **1992**, *30*, 19–48.
46. Passaglia, E.; Rinaldi, R. Katoite, a new member of the $Ca_3Al_2(SiO_4)_3$-$Ca_3Al_{12}(OH)_{12}$ series and a new nomenclature for the hydrogrossular group of minerals. *Bull. Minéral.* **1984**, *107*, 605–618.
47. Bailey, S.W.; Lister, J.S. Structures, compositions, and X-ray diffraction identification of dioctahedral chlorites. *Clays Clay Miner.* **1989**, *37*, 193–202.
48. Weiss, Z. Interpretation of chemical composition and X-ray diffraction patterns of chlorites. *Geol. Carpathica* **1991**, *42*, 93–104.
49. Bailey, S.W. (Ed.) Chlorites: Structures and crystal chemistry. In *Hydrous Phyllosilicates*; Reviews in Mineralogy; Mineralogical Society of America: Madison, WI, USA, 1988; Volume 19, 347–398.
50. Hey, M.H. A new review of the chlorites. *Mineral. Mag.* **1954**, *30*, 277–292.
51. Wicks, F.J.; Zussman, J. Microbeam X-ray diffraction patterns of the serpentine minerals. *Can. Mineral.* **1975**, *13*, 244–258.
52. Whittaker, E.J.W.; Zussman, J. The characterization of serpentine minerals by X-ray diffraction. *Mineral. Mag.* **1956**, *31*, 107–126.
53. Whittaker, E.J.W.; Wicks, F.J. Chemical differences among the serpentine "polymorphs". *Am. Mineral.* **1970**, *55*, 1025–1047.
54. Wada, K.; Yamada, H. Hydrazine intercalation-intersalation for differentiation of kaolin minerals from chlorites. *Am. Mineral.* **1968**, *53*, 334–339.
55. Franco, F.; Ruiz Cruz, M.D. A comparative study of the dehydroxylation process in untreated and hydrazine-deintercalated dickite. *J. Therm. Anal. Calorim.* **2006**, *85*, 369–375.

56. Bish, D.L.; Johnston, C.T. Rietveld refinement and Fourier-transform infrared spectroscopic study of the dickite structure at low temperature. *Clays Clay Miner.* **1993**, *41*, 297–304.
57. Merlino, S. Okenite, $Ca_{10}Si_{18}O_{46}{\cdot}18H_2O$: The first example of a chain sheet silicate. *Am. Mineral.* **1983**, *68*, 614–622.
58. Effenberger, H.; Mereiter, K.; Zemann, J. Crystal structure refinements of magnesite, calcite, rhodochrosite, siderite, smithsonite and dolomite, with discussion of some aspects of the stereochemistry of calcite-type carbonates. *Z. Kristallogr.* **1981**, *156*, 233–243.
59. McConnell, J.D.C. A chemical, optical and X-ray study of scawtite from Ballycraigy, Larne, N. Ireland. *Am. Mineral.* **1955**, *40*, 510–514.
60. Bentor, I.K.; Gross, S.; Heller, L. Some unusual minerals from the "Mottled Zone" complex, Israel. *Mineral. Mag.* **1963**, *48*, 924–930.
61. Ruiz Cruz, M.D.; Moreno Real, L. Practical determination of allophane and synthetic alumina and iron oxide gels by X-ray diffraction. *Clays Clay Miner.* **1991**, *26*, 377–387.
62. Pertsev, N.N. Skarns as magmatic and postmagmatic formations. *Int. Geol. Rev.* **1974**, *16*, 572–582.
63. Pertsev, N.N. *High-T Metamorphism and Metasomatism in Carbonate Rocks*; Nauka: Moscow, Russia, 1977; pp. 1–256. (In Russian).